5-2015

Vanadium trichloride thermochemical solar energy storage system analysis.

Caleb Michael Rogers
University of Louisville

VANADIUM TRICHLORIDE THERMOCHEMICAL SOLAR ENERGY STORAGE
SYSTEM ANALYSIS

By

Caleb Michael Rogers
B.S., University of Louisville, 2014

A Thesis
Submitted to the Faculty of the
University of Louisville
J.B. Speed School of Engineering
as Partial Fulfillment of the Requirements
for the Professional Degree

MASTER OF ENGINEERING

Department of Mechanical Engineering

May 2015

VANADIUM TRICHLORIDE THERMOCHEMICAL SOLAR ENERGY STORAGE
SYSTEM ANALYSIS

Submitted By: _____
Caleb Rogers

A Thesis Approved On

_____
(Date)

by the Following Reading and Examination Committee:

_____
Dr. Keith Sharp, Thesis Director

_____
Dr. Sam Park

_____
Dr. Eric Berson

ACKNOWLEDGEMENTS

ABSTRACT

As annual energy consumption grows, developing renewable solar energy conversion systems, storage systems, and high density electrical energy production systems is growing increasingly important. The proposed system utilizes vanadium trichloride thermal decomposition to produce chlorine gas and vanadium dichloride. A second reaction combines gaseous hydrogen chloride and the product vanadium dichloride to reform vanadium trichloride and produce hydrogen gas. Hydrogen gas and chlorine gas can be stored indefinitely and electrical energy is obtained from the chemicals by a non-humidified dry membrane hydrogen – chlorine fuel cell. The fuel cell produces the gaseous hydrogen chloride needed to reform vanadium trichloride. The cycle operates in a closed loop where vanadium trichloride is recycled.

Chemical equations and reaction kinetics are discussed for vanadium trichloride decomposition and synthesis. TRNSYS 16 software was used to evaluate the efficiency of the solar collection cycle with an SES parabolic dish Stirling collector in Louisville, KY and Phoenix, AZ. Thermodynamic calculations for the chemical reactions were performed. A dry membrane hydrogen – chlorine fuel cell model was developed from both theoretical calculations and experimental data (Liu, Zhou et al. 2013). The system efficiency was evaluated for two fuel cell current densities of 0.039 A/cm^2 and 0.085 A/cm^2. The potential efficiency of the vanadium trichloride cycle was compared to efficiency values for thermal energy storage (TES), compressed air energy storage systems (CAES), vanadium flow battery (Battery), pumped hydro electrical storage (PHES), and thermochemical ammonia storage (NH$_3$), evaluated by Shakeri, et al. (2014). All systems, with the exception of the vanadium trichloride system, used a

Stirling engine for electric energy production. Short – term storage system efficiency, cumulative system efficiency, and long – term energy storage system efficiency were compared for each storage system.

The analysis found that the vanadium trichloride cycle offers a significant advantage over other storage systems. The highest efficiency obtained was 39.3%, which was significantly higher than TES systems at 22.8% and the NH_3 system at 19.3%. Despite the difference in climate, system efficiency was decreased by only 1.3% in Louisville, KY when compared to Phoenix, AZ. The efficiency difference was due to a lower collector and receiver efficiency in Louisville than in Phoenix.

In addition, the vanadium trichloride system had a lower efficiency of energy to storage than both the TES and NH_3 cycles. Energy production from the vanadium trichloride system remained more efficient due to the high efficiency of the hydrogen – chlorine fuel cell, giving the vanadium trichloride system the overall advantage.

A comparison of the long – term energy storage efficiency of the systems showed that the vanadium trichloride system had a significant advantage over other storage and energy production systems. After seven months of continuous energy storage, the TES system efficiency reduced to 0.58%, the NH_3 system efficiency reduced to 18.7%, and the vanadium trichloride system efficiency reduced to 38.1%. The ability to store energy for long periods of time with low losses gives the vanadium trichloride system a significant advantage.

TABLE OF CONTENTS

NOMENCLATURE

H(T) = Enthalpy at temperature T

$H°_{298.15}$ = Standard state enthalpy at 298.15 K

$C_p(T)$ = Specific heat at temperature T

T = Temperature in Kelvin

$VCl_3(s)$ = Vanadium (III) chloride solid, vanadium trichloride solid

$VCl_2(s)$ = Vanadium (II) chloride solid, vanadium dichloride solid

$VCl_4(g)$ = Vanadium (IV) chloride gas, vanadium tetrachloride gas

$Cl_2(g)$ = Chlorine gas

HCl(g) = Hydrogen chloride gas

$H_2(g)$ = Hydrogen gas

ΔH_{FC} = Change in enthalpy of the fuel cell reaction

ΔS_{FC} = Change in entropy of the fuel cell reaction

ΔG_{FC} = Gibbs free energy change of the fuel cell reaction

E_{OCV} = Fuel cell open circuit voltage (OCV)

n = Number of transfer electrons

F = Faradays constant

η_R = Membrane resistance overpotential (V)

η_{H_2} = Hydrogen electrode overpotential (V)

η_{Cl_2} = Chlorine electrode overpotential (V)

j = Fuel cell operating current density

E = Operating voltage of the fuel cell

$P_{D,FC}$ = Operating power density of the fuel cell

$P_{in, collector}$ = Power into the collector (kW)

I_{DNI} = Direct normal incident solar radiation (kJ/s-m^2)

A_{proj} = Solar collector projected area (m^2)

$P_{out, collector}$ = Power out of the solar collector (kW)

ρ = Solar collector receiver reflectivity

φ_{wind} = Solar collector wind speed factor

φ_{shade} = Solar collector shading factor

$P_{out, receiver}$ = Power output of the receiver (kW)

$\dot{Q}_{r, r}$ = Receiver reflective radiation loss (kW)

$\dot{Q}_{cond}$ = Receiver conduction loss (kW)

$\dot{Q}_{conv, fr}$ = Receiver free convective loss (kW)

$\dot{Q}_{conv, fo}$ = Receiver forced convective loss (kW)

$\dot{Q}_{r, e}$ = Receiver loss due to emitted radiation (kW)

$\Delta H_{RX1}(T)$ = Heat of reaction for Reaction 1 at temperature T

$H_{VCl_2}(T)$ = Enthalpy of vanadium dichloride at temperature T

$H_{Cl_2}(T)$ = Enthalpy of chlorine gas at temperature T

$H_{VCl_3}(T)$ = Enthalpy of vanadium trichloride at temperature T

$\dot{Q}_{RX1}$ = Amount of solar power used for vanadium trichloride decomposition (kW)

x_d = Vanadium trichloride decomposition conversion efficiency

$\dot{n}_{VCl_3}$ = Molar flow rate of vanadium trichloride

$\dot{Q}_{HRX1}$ = The total power available from Reactor 1 products (kW)

C_{p, VCl_3} = Specific heat of vanadium trichloride

T_{RX1} = Temperature of vanadium trichloride decomposition in Reactor 1

$T_{O,RX2}$ = Temperature of reactants exiting Reactor 2

$T_{O,HRX2}$ = Temperature of vanadium chloride mixture exiting HRX2

T_{amb} = Ambient temperature

$\overline{T}$ = Average temperature of heat addition of removal

$\dot{n}_{VCl_2,i}$ = Molar flow rate of vanadium dichloride entering Reactor 1

$\dot{n}_{VCl_2}$ = Molar flow rate of vanadium dichloride exiting Reactor 1

C_{p, VCl_2} = Specific heat of vanadium dichloride

$\dot{n}_{Cl_2}$ = Molar flow rate of chlorine gas exiting Reactor 1

C_{p, Cl_2} = Specific heat of chlorine gas

T_{out, VCl_m} = Temperature of vanadium chloride mixture exiting HRX1 towards Reactor 1

ΔH_{ph1} = Amount of energy required by Preheater 1

$\dot{Q}_{HRX2, HCl}$ = The total power required to preheat hydrogen chloride gas (kW)

$\dot{Q}_{pc, VCl_m}$ = The total power required by the Precooler unit (kW)

x_s = Vanadium trichloride synthesis conversion efficiency

$\dot{n}_{VCl_2}$ = Molar flow rate of vanadium dichloride entering Reactor 2

$\dot{n}_{HCl}$ = Molar flow rate of hydrogen chloride gas entering Reactor 2

$\dot{n}_{r2,VCl_3}$ = Molar flow rate of vanadium trichloride exiting Reactor 2

$\dot{n}_{r2, H_2}$ = Molar flow rate of hydrogen gas exiting Reactor 2

$\dot{n}_{r2,HCl}$ = Molar flow rate of hydrogen chloride gas exiting Reactor 2

$\dot{n}_{H_2}$ = Molar flow rate of hydrogen gas into the fuel cell

$\dot{n}_{Cl_2}$ = Molar flow rate of chlorine gas into the fuel cell

$\Delta H_{RX2}(T)$ = Heat of reaction for Reaction 2 at temperature T

A_{active} = Fuel cell active area

λ = Fuel cell stoichiometric fuel supply ratio

T_{FC} = Fuel cell operating temperature

$\dot{Q}_{HRX3, HCl}$ = Power available from hydrogen chloride gas exiting the fuel cell (kW/cm^2)

$\dot{n}_{HCl,FC}$ = Molar flow rate of hydrogen chloride exiting the fuel cell

$T_{O,HRX3}$ = Temperature of hydrogen and chlorine gas exiting HRX3

$\dot{Q}_{ph2}$ = Power required by Preheater 2 (kW)

t = Total fuel cell run time

n_{H_2} = Amount of hydrogen gas available in storage

$Q_{out, FC}$ = Total energy output from the fuel cell (W-hr)

η_{thermo} = Thermodynamic efficiency of the fuel cell

η_c = Solar collector efficiency

η_r = Solar receiver efficiency

η_{RX} = Chemical reaction efficiency

η_{FC} = Hydrogen – chlorine fuel cell efficiency

η_{RX} = Efficiency of energy conversion from chemical reactions

$P_{RX,stored}$ = The amount of power stored from chemical reactions (kW)

$Q_{in,\ collector}$ = Total energy input to the solar collector (W-hr)

t_{step} = Simulation time step

LIST OF TABLES

LIST OF FIGURES

I.   INTRODUCTION

As world population continues to grow and per capita energy consumption rises, dependence on fossil fuels grows exponentially. It has been theorized that large dependence on fossil fuels will result in a climate degradation of earth, causing uninhabitable conditions. The depleting supply of fossil fuels drives the cost of energy higher. A shift from fossil fuels to renewable energy sources for primary energy load is necessary for both economic and climatic wellbeing. As of 2012, around 81% of energy produced in the United States originated from fossil fuels, 8% from nuclear energy, and 9% from renewable energy sources (U.S. Energy Information Administration 2012). Energy production figures have changed since 2012 to 39% electricity production from coal, 27% from natural gas, 19% from nuclear energy, 1% from petroleum, and 13% from renewable energy sources. Renewable electrical production is comprised of 52% from hydroelectric, 32% from wind, 8% from biomass wood, 4% from biomass waste, 3% from geothermal sources, and just 2% from solar energy sources (U.S. Energy Information Administration 2013). More progress with using solar energy sources is necessary to increase the renewable energy supply.

The primary source of renewable energy is in the form of incident radiation the earth receives from the sun. Converting renewable energy into electrical energy is a topic of growing interest. The large amount of energy that the earth receives daily from the sun exceeds the daily load in the United States by at least three orders of magnitude, but the duration of energy usage exceeds the daytime availability of solar energy. It is important to develop energy storage systems to store converted energy obtained from the sun. One option is to store energy during the day, and produce electrical energy during the night to

supply the load when the sun is present. Various options for the conversion of energy have been researched in the past. Large amounts of research has been performed on photovoltaics and utilizing hydrogen obtained by solar-powered water splitting for use in hydrogen – oxygen fuel cells.

Little research has been performed on the combination of various renewable energy systems; seen as the solution to energy conversion and storage. The proposed system utilizes vanadium (III) chloride decomposition and synthesis, performed with parabolic dish collectors, to produce chlorine gas and hydrogen gas. The products can be stored indefinitely and used with hydrogen - chlorine fuel cells to produce electrical energy as needed. The cycle operates as a closed system where reaction products are recycled through the system to reform the initial reactant.

Research of the decomposition temperature of vanadium (III) chloride was performed by Yajima (1979). An analysis of a vanadium (III) chloride process was presented in a patent by Amendola (2010). The analysis indicated that decomposition of vanadium (III) chloride could be obtained at relatively low temperatures between 423 K and 633 K with adequate conversion efficiencies.

Hydrogen – chlorine fuel cells have been researched since the 1970s when membrane material properties were little developed. As knowledge of membrane material properties has expanded, more recent research was performed by Magnus Thomassen at Harvard University (2006). Additional research into hydrogen – chlorine fuel cells performed by Harvard University yielded high efficiencies (Huskinson, Marshak et al. 2014). To the knowledge of the author, no research has been conducted on the combination of these systems for solar energy storage and electrical energy production.

The layout of the proposed system and chemical properties will be discussed, the methods utilized for analysis will be presented, a comparison of the results to other storage methods will be presented, and key implications of analysis findings will be discussed.

II.   SYSTEM DESCRIPTION

The analysis was completed with assumptions that will be discussed in more detail later in this section. To justify the assumptions, it is necessary to present a detailed description of chemical properties and the chemical reactions occurring in the closed loop cycle.

A. Cycle Description

The cycle is closed loop, and the initial reactant is reformed through a series of additional reactions (FIGURE 1). The cycle begins with solar energy concentration onto a receiver, increasing its temperature. Heat transfer fluid flowing through the receiver transfers energy to the first reactor vessel. A continuous flow reactor is most conducive to continuous operation (Amendola 2010).
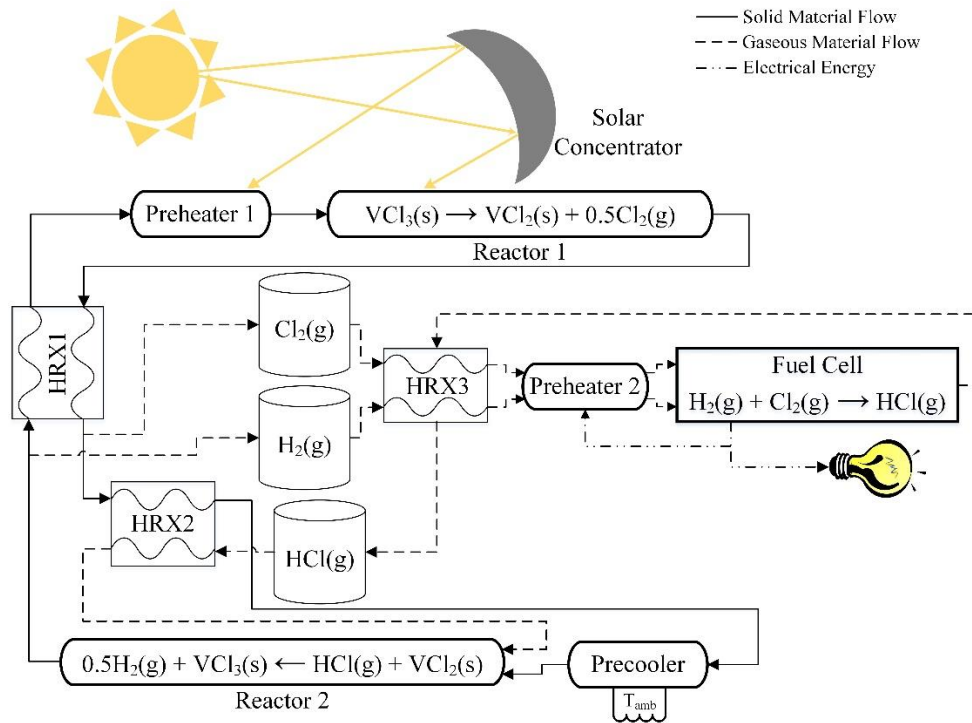
FIGURE 1 - Vanadium Chloride System Schematic

4

Preheater 1 supplies the necessary solar energy to heat the incoming vanadium (III)

chloride (VCl_3) to the reaction temperature. In Reactor 1, the concentrated solar energy is

used to heat vanadium (III) chloride, producing chlorine gas (Cl_2) and vanadium (II)

chloride solid (VCl_2). The products are used to increase the temperature of the incoming

VCl_3(s) through a counter flow heat recovery heat exchanger (HRX1 in FIGURE 1).

Chlorine gas is stored for energy production and vanadium (II) chloride is sent to HRX2.

The temperature of incoming hydrogen chloride gas to Reactor 2 is increased with heat

recovered from vanadium (II) chloride exiting HRX1. The second heat recovery process

occurs in HRX2. Hydrogen chloride gas (HCl), is obtained from the hydrogen – chlorine

fuel cell when electricity is produced. The temperature of the incoming vanadium (II)

chloride is further reduced with the Precooler unit where energy is released to the

surroundings. VCl_2(s) and HCl(g) are combined in Reactor 2 to form VCl_3(s) and

hydrogen gas (H_2).

Chlorine gas from Reaction 1 and hydrogen gas from Reaction 2 can be stored

indefinitely and used to produce electrical energy from the hydrogen – chlorine fuel cell.

The temperature of the incoming gasses is increased through HRX3 by the output

hydrogen chloride gas from the fuel cell. Additional heat is supplied to the incoming

gasses by Preheater 2, where electrical energy is provided by the fuel cell. The product of

the fuel cell is HCl(g), which is stored until needed for use in Reactor 2.

Compression and expansion of gasses between reaction pressure and storage

pressure have been neglected. Optimum efficiency would be promoted by a system

design that minimizes these pressure differences. High-pressure storage leakage is

estimated at around 0.5% per year (Harvey 1995). One method of low pressure storage is

with underground salt mines and caverns. Underground cavern leakage has been estimated around 0.37% per year (Harvey 1996). An annual leakage of 0.5% was used for the vanadium cycle.

<center>B. Chemical Properties</center>

Enthalpy, specific heat, and entropy of hydrogen gas (H_2), chlorine gas (Cl_2), hydrogen chloride gas (HCl), vanadium (II) chloride (VCl_2), and vanadium (III) chloride (VCl_3) were obtained from previous experimental data. Enthalpy, entropy, and specific heat as a function of temperature for hydrogen gas, chlorine gas, and hydrogen chloride gas were obtained from the NIST Chemistry WebBook database (2005) and are characterized, respectively, with the Shomate Equation by

$$H(T) - H^\circ_{298.15} = A(T) + B\left(\frac{T^2}{2}\right) + C\left(\frac{T^3}{3}\right) + D\left(\frac{T^4}{4}\right) - \frac{E}{T} + F - H \qquad (1)$$

$$S(T) = A[\ln T] + B(T) + C\left(\frac{T^2}{2}\right) + D\left(\frac{T^3}{3}\right) - \frac{E}{(2T^2)} + G \qquad (2)$$

$$C_p(T) = A + B(T) + C(T^2) + D(T^3) + \frac{E}{t^2} \qquad (3)$$

where T is equal to the temperature of the species in units of Kelvin divided by 1000, H is enthalpy in units of kJ/mole, S is entropy in units of J/mole-K, and C_p is specific heat in units of J/mole-K. Coefficients A, B, C, D, E, F, H, and G for hydrogen gas, chlorine gas, and hydrogen chloride gas are shown in TABLE I.

<center>6</center>

TABLE I

SHOMATE EQUATION COEFFICIENTS FROM NIST DATABASE

Species	Hydrogen, $H_2(g)$	Chlorine, $Cl_2(g)$	Hydrogen chloride, $HCl(g)$
A	33.066178	33.05060	32.12392
B	-11.363417	12.22940	-13.45805
C	11.432816	-12.06510	19.86852
D	-2.772874	4.385330	-6.853936
E	-0.158558	-0.1594940	-0.049672
F	-9.980797	-10.83480	-101.6206
G	172.707974	259.02900	228.6866
H	0.000000	0.00000	-92.31201

Coefficient data given in TABLE I is valid for the temperature range of 298 K to 1000 K for hydrogen gas, 298 K to 1000 K for chlorine gas, and 298 K to 1200 K for hydrogen chloride gas (National Institute of Standards and Technology 2005).

Enthalpy, and specific heat as a function of temperature for vanadium (II) chloride (VCl_2) and vanadium (III) chloride (VCl_3) were obtained from data collected by King et al. (1948). Enthalpy and specific heat as a function of temperature for vanadium (II) chloride are characterized, respectively, by

$$H(T) - H°_{298.15} = (17.25)T + (1.36 \times 10^{-3})T^2 + (0.71 \times 10^5)T^{-1} - 5502 \qquad (4)$$

$$C_p(T) = 17.25 + (2.72 \times 10^{-3})T - (0.71 \times 10^5)T^{-2} \qquad (5)$$

where T is the temperature in Kelvin of vanadium (II) chloride valid for temperatures from 298 K to 1200 K, H is enthalpy in units of calories/mole, and C_p is specific heat in units of calories/mole-K. Enthalpy and specific heat as a function of temperature for vanadium (III) chloride are characterized, respectively, by

$$H(T) - H°_{298.15} = (22.99)T + (1.96 \times 10^{-3})T^2 + (1.68 \times 10^5)T^{-1} - 7592 \qquad (6)$$

$$C_p(T) = 22.99 + (3.92 \times 10^{-3})T - (1.68 \times 10^5)T^{-2} \qquad (7)$$

where T is the temperature in Kelvin of vanadium (III) chloride valid for a temperatures

from 298 K to 900 K, H is enthalpy is in units of calories/mole, and C_p is specific heat in

units of calories/mole-K. Entropy values for vanadium (II) chloride and vanadium (III)

chloride at various temperatures are given in TABLE II (King 1948).

TABLE II

VANADIUM CHLORIDE COMPOUND ENTROPY DATA

Species	Vanadium (II) Chloride	Vanadium (III) Chloride
Temp. (K)	S_T-$S_{298.15}$ (cal./mol-K)	S_T-$S_{298.15}$ (cal./mol-K)
400	5.30	6.80
500	9.27	12.09
600	12.61	16.55
700	15.50	20.43
800	18.07	23.85
900	20.36	26.90
1000	22.45	
1100	24.36	
1200	26.13	
1300	27.77	

Entropies at various temperatures were found using a curve fit of data from TABLE II.

The resulting curves produced an R^2 value of 1.000 indicating that the curves closely

matched the experimental data.

<center>C. Description of Chemical Reactions</center>

The system utilizes solar-powered thermal decomposition of vanadium (III) chloride to vanadium (II) chloride and chlorine gas as a mechanism of chlorine gas production. Chlorine gas is then stored indefinitely to be combined with hydrogen gas to produce electrical energy from a hydrogen - chlorine fuel cell. The output from the fuel cell is hydrogen chloride gas, which is stored for use in Reaction 2.

In the second reactor, vanadium (II) chloride is combined with hydrogen chloride gas to reform vanadium (III) chloride and produce hydrogen gas. The hydrogen gas is stored for use in the fuel cell, and vanadium (III) chloride is recycled to start the process over.

1. Reaction 1

Reactor 1 (FIGURE 1) was operated at a temperature of 898 K, further explained in the next section. In Reactor 1, the thermal decomposition of vanadium (III) chloride is characterized by

$$2VCl_3(s) + \Delta H_R \rightarrow VCl_2(s) + VCl_4(g) \tag{8}$$

where $VCl_2(s)$ is vanadium (II) chloride, $VCl_4(g)$ is vanadium (IV) chloride formed in the gaseous state, and ΔH_R is the heat of reaction equal to 184.1 kJ/mole. The reaction is endothermic and requires energy input for an ongoing reaction. The reaction begins to occur at 623 K and ends at 923 K (Yajima, Matsuzaki et al. 1979). However, $VCl_4(g)$ is decomposed at temperatures in the 423 K to 473 K range (Simons and Powell 1945).

<center>9</center>

Thus, the $VCl_4(g)$ will be decomposed immediately into $VCl_3(s)$ and $Cl_2(g)$, characterized by

$$VCl_4(g) + \Delta H_R \rightarrow VCl_3(s) + \frac{1}{2}Cl_2(g) \tag{9}$$
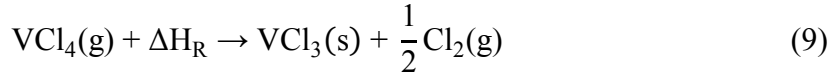
where $Cl_2(g)$ is the chlorine gas produced, and ΔH_R is the heat of reaction equal to -55.23 kJ/mole. Because the heat of reaction is negative, energy is released from the reaction in an exothermic manner. The resulting $VCl_3(s)$ is immediately available for Reaction 1 according to Equation 8, which again provides $VCl_4(g)$ for the secondary reaction given in Equation 9, and so on.

From Equations 8 and 9, it is seen that $VCl_4(g)$ is an intermediary of the decomposition reaction. It is expected that little $VCl_4(g)$ will escape the reactor due to its low decomposition temperature. Therefore, decomposition of $VCl_3(s)$ can be characterized, with reasonable accuracy, by combining Equations 8 and 9 for

$$VCl_3(s) + \Delta H_R \rightarrow VCl_2(s) + \frac{1}{2}Cl_2(g) \tag{10}$$
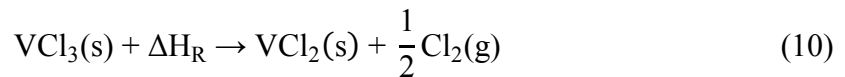
which is a model applied in prior research (Amendola 2010). ΔH_R in Equation 10 is the heat of reaction equal to 128.87 kJ/mole at 298.15 K and 124.45 kJ/mole at a temperature of 898 K. The reaction is endothermic and energy is required to sustain an ongoing reaction.

The solid products of Reaction 1, characterized by Equation 10, are $VCl_2(s)$ in addition to some unreacted $VCl_3(s)$ due to imperfect conversion efficiency of the chemical reaction.

2. Reaction 2

The solid products of Reaction 1 are transferred to Reactor 2 (FIGURE 1) for hydrogen gas production. Reactor 2 was operated at a temperature of 393 K, explained further in the next section. The chemical reaction that occurs in Reactor 2 is characterized by

$$VCl_2(s) + HCl(g) + \Delta H_R \rightarrow VCl_3(s) + \frac{1}{2}H_2(g) \qquad (11)$$
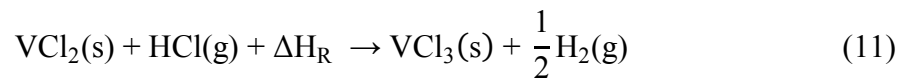
where $VCl_3(s)$ is reformed, $H_2(g)$ is produced, and ΔH_R is the heat of reaction equal to -36.56 kJ/mole at 298.15 K and -35.83 kJ/mole at 393 K. Reaction 2 is exothermic meaning it releases energy to the products during the reaction. Due to imperfect conversion efficiency, Reaction 2 solid products are $VCl_3(s)$ in addition to some $VCl_2(s)$. Gaseous products are $H_2(g)$, in addition to some $HCl(g)$. Hydrogen gas and hydrogen chloride gas are separated and stored, while $VCl_3(s)$ and $VCl_2(s)$ are recycled back to Reactor 1, starting the process over. The result of the reactions is the production of hydrogen gas and chlorine gas, which can be stored indefinitely until electrical energy is needed.

3. Reaction Kinetics

The thermal decomposition of vanadium (III) chloride, characterized by Reaction 1 (Equation 10), is not well documented in literature. Although chemical analyses of vanadium (III) chloride decomposition have been performed, the conversion efficiency and reaction rate for decomposition of vanadium (III) chloride are not characterized. There are discrepancies in vanadium (III) chloride decomposition data collected by Thermogravimetric (TG) analysis from Yijuma et al. (1979) and Amendola (2010). In this analysis, the conversion efficiency of Reaction 1 at a temperature of 898 K was characterized by data obtained from Yijuma et al. (1979). In order to accurately characterize the system efficiency, the reaction rate and conversion efficiency at various temperatures for Reaction 1 and Reaction 2 must be further researched (Amendola 2010).

Graphical data from Yijuma et al. (1979) indicates that Reaction 1 (Equation 10) is complete around 898 K. Reaction 1 is known in literature to take place rapidly at 898 K (Knoche and Schuster 1984). In addition, temperatures above 973 K further decompose $VCl_2(s)$ resulting in the product vanadium, which is undesirable (Yajima, Matsuzaki et al. 1980). Ideal conversion efficiencies for Reaction 2 are in the temperature range of 898 K and 950 K. Therefore, simulations for vanadium (III) chloride decomposition were performed at a temperature of 898 K, assuming that an ideal 90% conversion efficiency is achieved. Ideal conversion efficiency may be achieved through the use of a catalyst (Amendola 2010).

Reaction 2 has little documentation in literature. It is suggested in literature that Reaction 2 is not in a desired state of equilibrium (Knoche and Schuster 1984). The use of a catalyst for Reaction 2 could improve the equilibrium state and increase the

12

conversion efficiency. Reaction 2 temperatures vary widely in literature. Temperatures

for Reaction 2 range in literature from 298 K by Stewart (2007) and Funk (1976), to 393

K by Lewis et al. (2009). Because the aim of this study was to determine the maximum

potential efficiency of the system, an ideal conversion efficiency of 90%, assuming the

use of a catalyst, and a temperature of 393 K was used for Reaction 2 simulations.

However, in light of the uncertainty for the conversion efficiency of Reaction 2, two

additional simulations were performed: the first with varying conversion efficiency from

0% to 90% to show the effect on overall efficiency, and the second with a conversion

efficiency of 45% for comparison to thermal energy storage (TES), compressed air

energy storage systems (CAES), vanadium flow battery (Battery), pumped hydro

electrical storage (PHES), and thermochemical ammonia storage (NH_3) systems.

D. Description of Energy Production

Energy is produced with hydrogen gas and chlorine gas from a hydrogen - chlorine

fuel cell by

$$H_2(g) + Cl_2(g) + \Delta H_R \rightarrow 2HCl(g) \tag{12}$$
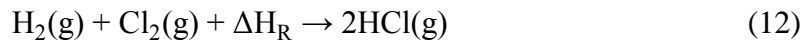
where $HCl(g)$ is stored for use in Reaction 2 (Equation 11), and ΔH_R is discussed further

later in this section. Harvard University has performed research into hydrated

regenerative hydrogen chlorine fuel cells (rHCFC), where the product of the fuel cell is

an aqueous solution of hydrogen chloride $HCl(aq)$ (Rugolo, Huskinson et al. 2012). From

their research, it was found that dehydration of the membrane leads to sub-optimal

operating conditions. Having a circulating water stream, which functions as both a coolant and as a hydrator for the cathode side of the membrane, was necessary for increasing fuel cell performance. The fuel cell must also be supplied with $Cl_2(l)$ between 12 psig and 75 psig (Huskinson, Marshak et al. 2014). Because the vanadium chloride system operates at low pressures, the compression and expansion steps needed for the chlorine stream would cause a reduction in system efficiency. In addition, it is seen from Reaction 2 (Equation 11) that using HCl(aq) in Reactor 2 will produce VCl_3(aq), requiring additional energy input to Reaction 1 to dehydrate VCl_3(aq) to VCl_3(s). The system can run as a wet cycle, but efficiencies are expected to be lower due to the need for dehydrated VCl_3(s) for Reaction 1.

More recent research has been performed on a hybrid membrane hydrogen - chlorine fuel cell (Liu, Zhou et al. 2013) that uses a porous nano-filtration membrane doped with proton conducting ionic liquids (NF/IL). The hybrid membrane allows the fuel cell to operate at high temperatures without hydration. The ionic liquid chosen for the nano-filtration membrane was trimethylammonium phosphate, ($[N_{1,1,1}H]H_2PO_4$). This type of fuel cell allows for the production of HCl(g) directly. Liu et al. (2013) operated the fuel cell at 393 K, 413 K, and 433 K with low change in the open circuit voltage. In addition, the nano-filtration membrane fuel cell operating in the temperature range 393 K – 433 K showed no decomposition of the proton conducting ionic liquid. One drawback of this design is cooling and heating of the incoming H_2(g) and Cl_2(g). Storing H_2(g) and Cl_2(g) at ambient temperature requires heating of these gases to optimize fuel cell efficiency. The energy required to preheat the incoming gas is supplied from a counter flow heat recovery heat exchanger (HRX3 in FIGURE 1) and a preheating unit (Preheater

2 in FIGURE 1). The high temperature will cause losses from the fuel cell to the

atmosphere if the stack is not well insulated. The fuel cell operates with a closed reactant

stream resulting in hydrogen chloride gas as the single product. This eliminates the need

to separate the unreacted gas from the product hydrogen chloride gas prior to storage. For

the analysis, a hydrogen - chlorine fuel cell operating temperature of 393 K was used.

Theoretical calculations were performed to evaluate the open circuit voltage, OCV

(E_{OCV}), of the non-humidified hydrogen – chlorine fuel cell operating at 393 K. The

change in enthalpy for the fuel cell reaction (Equation 12) was found using

$$\Delta H_{FC} = H_{Products} - H_{Reactants} \tag{13}$$

where H is enthalpy of each species at a temperature of 393 K and calculated in

kJ/kmole. The calculated enthalpy for the fuel cell reaction is equal to -185167.1

kJ/kmole. The change in entropy for the fuel cell reaction (Equation 12) was found using

$$\Delta S_{FC} = S_{Products} - S_{Reactants} \tag{14}$$

where S is the entropy of each species evaluated at a temperature of 393 K and calculated

in kJ/kmole-K. The calculated entropy for the fuel cell reaction is equal to 18.48996

kJ/kmole-K. Gibbs free energy change was found from the calculated enthalpy and

entropy using

$$\Delta G_{FC} = \Delta H_{FC} - T\Delta S_{FC} \tag{15}$$

15

where ΔH is the change in enthalpy in units of kJ/kmole, T is the fuel cell operating temperature equal to 393 K, and ΔS is the change in entropy in units of kJ/kmole-K. The calculated Gibbs free energy change at 393 K for the fuel cell reaction (Equation 12) is equal to -192526.1 kJ/kmole.

The open circuit voltage, E_{OCV}, was found using

$$E_{OCV} = \frac{-\Delta G}{nF} \tag{16}$$

where ΔG is the Gibbs free energy change in units of kJ/kmole at a temperature of 393 K, n is the number of exchange electrons equal to 2, and F is Faradays constant given as 96485.3 C/mole. The unit C represents coulombs defined as the amount of electrical charge transported through a constant current of one ampere in one second (Wikipedia Contributors 2015). The theoretical OCV was calculated to be 0.9972 V, which was used in conjunction with experimental data collected by Sa Liu et al. (2013) to produce a model based on both experimental data and theoretical calculations for fuel cell operation at 393 K.

Fuel cell operating voltage is lower than the OCV due to the fuel cell activation energy loss and overpotential losses. The fuel cell overpotentials contribute to the loss of fuel cell potential leading to the production of heat (Rugolo 2011). The operating fuel cell potential as a function of operating current was defined as

$$E(j) = E_{ocv} - \eta_R(j) - \eta_{H_2}(j) - \eta_{Cl_2}(j) \tag{17}$$

where η_R is the membrane resistance overpotential in volts, η_{H_2} is the hydrogen electrode overpotential in volts, η_{Cl_2} is the chlorine electrode overpotential in volts, and j is the operating current density of the fuel cell. Because dry hydrogen-chlorine fuel cells with hybrid membranes have little documentation, it is difficult to characterize the losses associated with the activation energy, membrane resistance, hydrogen gas electrode resistance, and chlorine gas electrode resistance. However, experimental data of voltage and power density versus current density show distinct trends where activation energy losses, membrane resistance, and electrode overpotential losses are present. Membrane resistance overpotential losses and electrode overpotential losses show a linear decaying trend. At low current densities, activation energy losses are present and follow a parabolic trend. To characterize the overpotential and activation energy losses within the hydrogen − chlorine fuel cell model, data from Sa Liu et al. (2013) for fuel cell operation at 393 K was plotted and a curve fit for voltage and power density versus current density was calculated. The y-axis intercept for voltage versus current density corresponds to the OCV of the fuel cell. In order to model the fuel cell from theoretical calculations and experimental data, the calculated theoretical OCV was used as the y-axis intercept in the curve fit equation. The operating voltage versus current density for the hydrogen − chlorine fuel cell model is

$$E(j) = (-30867)j^5 + (15161)j^4 - (2866)j^3 + (260.78)j^2 - (16.175)j + 0.9972 \qquad (18)$$

where j is the operating current density of the fuel cell in A/cm^2, and E(j) is calculated in volts. Equation 18 produced a close fit to the evaluated data points with an R^2 value of 1.00. The operating power density versus current density for the fuel cell model was found using

$$P_{D,FC}(j) = (901.7)j^5 - (390.8)j^4 + (62.01)j^3 - (8.910)j^2 + (0.8985)j + 0.0002 \quad (19)$$

where E(j) is the operating voltage of the fuel cell in volts, and j is the operating current density of the fuel cell in A/cm^2. Equation 19 produced a close fit to the evaluated data points with an R^2 value of 0.9998.

The voltage and power density versus current density (Equation 18 and Equation 19) for the fuel cell model are shown in FIGURE 2.
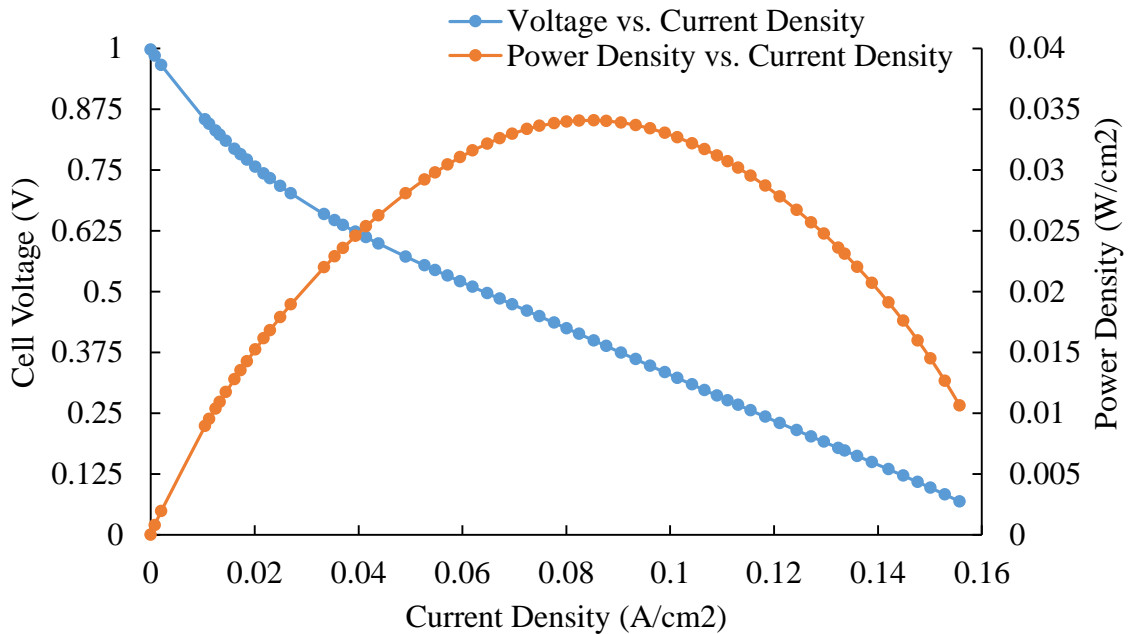
FIGURE 2 - Fuel Cell Model Based From Theoretical And Experimental Data

Data from FIGURE 2 was used to determine the current densities for the evaluation of fuel cell performance. The first fuel cell operating condition was chosen where there is a balance between operating voltage and current density, corresponding to the intersection of the voltage and power density curves. Beyond this point, high overpotential losses from the hydrogen and chlorine electrodes lower fuel cell performance. The second fuel cell operating condition was chosen where the power density is highest, corresponding to the peak of the power density versus current density curve. Current densities higher than that of the maximum power density result in very low fuel cell performance. The first operating condition was evaluated for a voltage of 0.6228 V and a current density 0.0394 A/cm^2. The second operating condition was evaluated for a voltage 0.3993 V and a current density of 0.0853 A/cm^2.

III.   METHODS

A. Analysis Method

System efficiency was calculated and compared to that of other energy storage and
conversion systems evaluated by a previous University of Louisville research project
performed by Shakeri et al. (2014). The other systems were thermal energy storage
(TES), compressed air energy storage systems (CAES), vanadium flow battery (Battery),
pumped hydro electrical storage (PHES), and thermochemical ammonia storage (NH_3).
All systems were compared in Phoenix, Arizona and Louisville, Kentucky. Phoenix has
primarily clear skies and Louisville has a greater number of overcast and cloudy days.
The comparison depicts typical Southwest conditions and typical Midwest conditions to
characterize a range of possible efficiencies. Analysis of the parabolic solar dish collector
for the system was performed using typical meteorological year (TMY3) weather data in
TRNSYS 16 (Klein et al. 2004). TMY3 weather data was obtained from the National
Renewable Energy Laboratory (2015). A parabolic dish Stirling collector from SES was
used to supply the system with solar energy. Thermochemical analyses were performed
in Microsoft Excel (2013). The overall efficiency of the system was also analyzed in
Excel and is presented in the results section.

B. TRNSYS 16 Description

TRNSYS (TRaNsient SYstem Simulation) is an energy simulation program
developed by the University of Wisconsin (Klein et al. 2004). TRNSYS has, for instance,
been used to produce accurate simulations of SEGS solar power plants when compared to

measured data (Stuetzle 2002). Parabolic trough collectors have a distinct economic advantage over parabolic point focus collectors due to their low cost. Currently, the highest attainable operating temperatures of parabolic trough collectors are between 673 K and 773 K (Fernández-García, Zarza et al. 2010), which is too low for efficient vanadium (III) chloride decomposition. Consequently, a parabolic point focus collector was used for the system analysis. The collector is a two-axis tracking system (Stirling Energy Systems (SES), Scottsdale, AZ) having a projected area of 41.1 m^2, reflectivity of 0.91, receiver absorber area of 0.6 m^2, and cavity diameter of 0.2 m. Collector and receiver losses result from free convection and emitted radiation to ambient conditions. The free convection and emitted radiation losses for the receiver result from the average receiver temperature. The TRNSYS model used for the simulation is viewed in FIGURE 3.
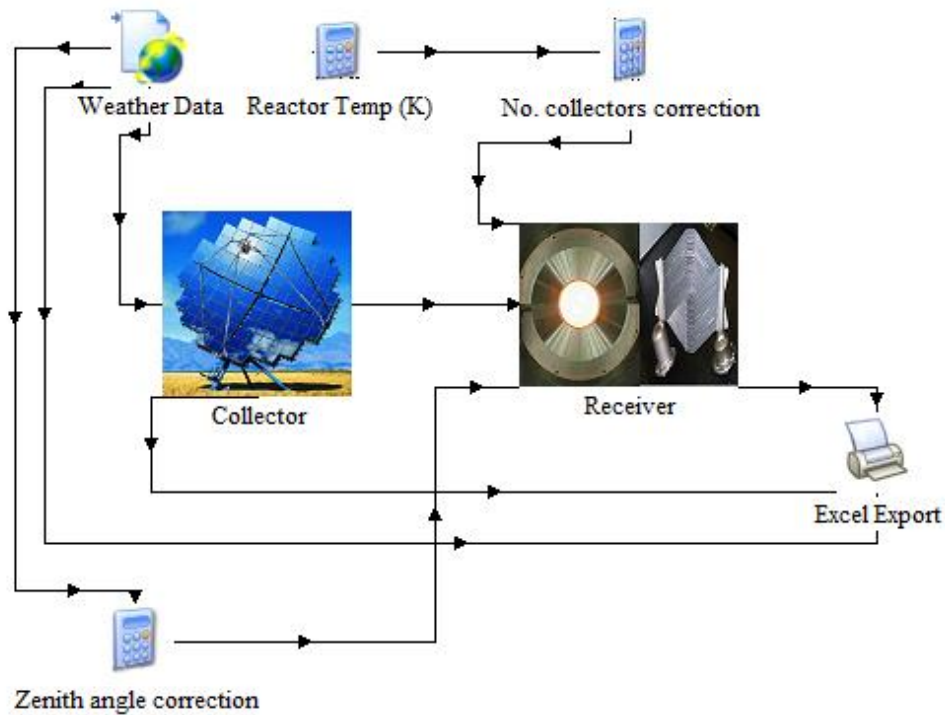
FIGURE 3 - TRNSYS Model Used For Simulations

The TRNSYS model utilized a collector and receiver modeled from the SES parabolic dish collector previously mentioned. Weather data for Louisville and Phoenix was input to the collector component from an external TMY3 document. The weather data was converted from TMY3 format to TMY2 format for use in TRNSYS 16. Calculated energy from the collector was input to the receiver component. Solar power received by the collector, collector power loss, power out of the collector, power into the receiver, receiver power loss, power out of the receiver, and ambient temperature were output to an external Microsoft Excel (2013) spreadsheet from the Excel Export (FIGURE 3) component to calculate the performance of the system.

C. Solar Collection Simulation

Solar energy received by the SES collector is equivalent to the total power supplied to the system. The total power that enters the system through the parabolic dish collector was characterized using

$$P_{in,\ collector} = I_{DNI} A_{proj} \tag{20}$$

where I_{DNI} is the direct normal incident solar radiation supplied by TMY3 weather data, and A_{proj} is the parabolic collector projected area. Output power from the collector is characterized by

$$P_{out,\ collector} = P_{in,\ collector}(\rho)(\varphi_{wind})(\varphi_{shade}) \tag{21}$$

where ρ is the reflectivity of the collector mirrors, φ_{wind} is the wind speed factor, and φ_{shade} is the shading factor. The wind speed factor varies from 1, when wind speeds correspond to safe operating conditions, and 0, when wind speed exceeds the maximum operating wind speed where the receiver is stowed to prevent damage. The shading factor varies depending on how many collectors are in the solar field. The current study only utilizes one parabolic dish collector with a shading factor of 1. Power output of the receiver is defined as

$$P_{out, \, receiver} \; = \; P_{out, \, collector} - \dot{Q}_{r, \, r} - \dot{Q}_{cond} - \dot{Q}_{conv, \, fr} - \dot{Q}_{conv, \, fo} - \dot{Q}_{r, \, e} \qquad (22)$$

where $\dot{Q}_{r, \, r}$ is the loss due to reflected radiation, $\dot{Q}_{cond}$ is the loss due to conduction, $\dot{Q}_{conv, \, fr}$ is the loss due to free convection, $\dot{Q}_{conv, \, fo}$ is the loss due to forced convection, and $\dot{Q}_{r, \, e}$ is the loss due to the emitted radiation of the receiver. The emitted radiation and free convection terms are the major sources of energy loss from the receiver. Simulations of collector performance were performed in TRNSYS and output every 15 minutes of the year to an external Excel file to perform reactor simulations.

D. Reactor 1 Simulation

The chemical reaction occurring in Reactor 1 (FIGURE 1) is Reaction 1 (Equation 10), given in the previous section. The enthalpy of Reaction 1 at temperature T was found using

$$\Delta H_{RX1}(T) = H_{VCl_2}(T) + \frac{1}{2}H_{Cl_2}(T) - H_{VCl_3}(T) \tag{23}$$

where H_{VCl_2} is the enthalpy of vanadium (II) chloride at temperature T, H_{Cl_2} is the

enthalpy of hydrogen gas at temperature T, and H_{VCl_3} is the enthalpy of vanadium (III)

chloride at temperature T. Enthalpies where found using Equations 1, 4, and 6 for each

species (TABLE III).

TABLE III

ENTHALPIES FOR REACTION 1 SPECIES

Species	Enthalpy (kJ/mole)
$Cl_2(g)$	21.753
$VCl_2(s)$	-405.17
$VCl_3(s)$	-518.74

Using the enthalpy value of each species from TABLE III with Equation 23, the enthalpy

of reaction for Reaction 1 was calculated as 124.45 kJ/mole. Reaction 1 is endothermic,

meaning it requires energy input to sustain the reaction.

Due to the conversion efficiency of Reaction 1, some vanadium (III) chloride leaves

the reactor without decomposing. The total amount of solar power used to decompose

vanadium (III) chloride in Reactor 1 was found using

$$\dot{Q}_{RX1} = x_d \dot{n}_{VCl_3} \Delta H_{RX1}(T) \tag{24}$$

where x_d is the reaction conversion efficiency at temperature T, and $\dot{n}_{VCl_3}$ is the molar

flow rate of vanadium (III) chloride into the reactor. As previously stated, Reaction 1 was

evaluated at a temperature of 898 K where decomposition occurs rapidly and the conversion efficiency was assumed as 90%.

In order to increase the thermal efficiency of the system, a counter flow heat recovery heat exchanger (HRX1 in FIGURE 1) was used to heat incoming reactants to Reactor 1 temperature by the products of Reactor 1. Products from Reactor 1 are cooled from the temperature of Reaction 1 to the temperature of products from Reaction 2. The total power available from the hot products exiting Reactor 1 was found using

$$
\begin{aligned}
\dot{Q}_{HRX1} = [(1\text{-}x_d)\dot{n}_{VCl_3}C_{p,\ VCl_3}(\overline{T}) + \dot{n}_{VCl_2}C_{p,\ VCl_2}(\overline{T}) \\
+ \dot{n}_{Cl_2}C_{p,\ Cl_2}(\overline{T})](T_{RX1} - T_{O,RX2})
\end{aligned} \tag{25}
$$

where $\dot{n}_{VCl_2}$ is the molar flow rate of vanadium (II) chloride exiting Reactor 1, $\dot{n}_{Cl_2}$ is the molar flow rate of chlorine gas exiting Reactor 1, C_p is found for each species at temperature $\overline{T}$, and $\overline{T}$ is the average temperature between Reaction 1, T_{RX1}, and products from Reaction 2, $T_{O,RX2}$. The energy from the hot products increases the temperature of the incoming vanadium (III) chloride, in addition to small amounts of vanadium (II) chloride due to Reaction 2 conversion efficiency. The temperature of the vanadium (III) chloride and vanadium (II) chloride mixture exiting the heat recovery exchanger was found using

$$
T_{out,\ VCl_m} = \left(\frac{\dot{Q}_{HRX1}}{\dot{n}_{VCl_3}C_{p,\ VCl_3}(\overline{T}) + \dot{n}_{VCl_{2,i}}C_{p,\ VCl_2}(\overline{T})} \right) + T_{O,RX2} \tag{26}
$$

where C_p is evaluated at the average temperature between the entering and exiting temperature, and $\dot{n}_{VCl_2,i}$ is the molar flow rate of vanadium (II) chloride from Reactor 2. The energy recovered from the reaction products is not adequate to fully heat the incoming vanadium (III) chloride and vanadium (II) chloride mixture to the temperature of Reaction 1. Therefore, some solar energy is used in Preheater 1 (FIGURE 1) to raise the temperature of the incoming vanadium chloride mixture. Since the flow rate of vanadium (III) chloride through the reactor is initially unknown, a preliminary temperature must be guessed for $T_{out,\,VCl_m}$ to calculate the amount of solar energy required by Preheater 1. The amount of energy per unit molar flow rate of vanadium (III) chloride required by Preheater 1 was calculated using

$$\Delta H_{ph} = \left(C_{p,\,VCl_3}(\overline{T}) + (x_d)(1 - x_s)C_{p,\,VCl_2}(\overline{T}) \right) \left(T_{RX1} - T_{out,\,VCl_m} \right) \qquad (27)$$

where x_s is the conversion efficiency of Reaction 2, and C_p is evaluated at the average temperature for each species, $\overline{T}$, between $T_{RX,1}$ and $T_{out,\,VCl_3}$. The molar flow rate of the incoming vanadium (III) chloride that is capable of being decomposed from solar energy was calculated using

$$\dot{n}_{VCl_3} = \frac{P_{out,\,receiver}}{x_d \Delta H_{RX,\,1}(T) + \Delta H_{ph}} \qquad (28)$$

where $\dot{n}_{VCl_3}$ effects the amount of heat recovered in Equation 25. Since $T_{out,\,VCl_3}$ is initially guessed, multiple iterations of both reaction simulations are performed within

each time step until T_{out, VCl_3} converges to a single value for each time step. Reaction 1 and Reaction 2 were iterated together to appropriately characterize vanadium (II) chloride flow rate into Reactor 1, $\dot{n}_{VCl_2,i}$, and the temperature of the products from Reactor 2, $T_{O,RX2}$. The molar flow rate of chlorine gas and vanadium (II) chloride leaving Reactor 1 was calculated, respectively, using

$$\dot{n}_{Cl_2} = \frac{1}{2} x_d \dot{n}_{VCl_3} \qquad (29)$$

$$\dot{n}_{VCl_2} = x_d \dot{n}_{VCl_3} + \dot{n}_{VCl_2,i} \qquad (30)$$

where, after passing through HRX1, chlorine gas is sent to storage at ambient temperature, and vanadium (II) chloride, in addition to small amounts of vanadium (III) chloride, are sent to Reactor 2.

E. Reactor 2 Simulation

The chemical reaction occurring in Reactor 2 (FIGURE 1) is Reaction 2 (Equation 11). Reaction 2 is exothermic and releases energy to the products of the reaction. The energy released raises the temperature of the products. Reactor 1 and Reactor 2 run simultaneously. Reactor 2 requires hydrogen chloride gas to operate, which is supplied from storage. Thus, there must be a sufficient supply of hydrogen chloride gas in storage for continued operation of the reactor cycle. Running Reactor 1 and Reactor 2 simultaneously allows chlorine gas from Reactor 1 to exit HRX1 at the temperature of products exiting Reactor 2, around 648 K, and thermal energy is lost to the surroundings

from the chlorine storage vessel. Additionally, product hydrogen gas and small amounts of hydrogen chloride gas exiting Reactor 2 are stored at 648 K, further adding to thermal losses. If storage was sufficiently insulated, storage temperature can be maintained on a short-term basis allowing hydrogen and chlorine gas to enter the fuel cell without additional heating. Hydrogen chloride gas that is left unreacted and stored in insulated tanks around 648 K could also be supplied directly to Reactor 2 without additional heating. The equation used to find the temperature increase from the released exothermic energy is discussed later in this section.

The temperature of the incoming mixture of vanadium (II) chloride and vanadium (III) chloride to Reactor 2 is higher than the Reactor 2 operating temperature. A counter flow heat recovery heat exchanger (HRX2 in FIGURE 1) is used to transfer heat from the vanadium chloride mixture to the hydrogen chloride gas supplied to Reactor 2. Vanadium (II) chloride and vanadium (III) chloride undergo an additional cooling process in the Precooler unit (FIGURE 1) to reduce their exiting temperature from HRX2 to the temperature of Reactor 2. From Reaction 2 (Equation 11), hydrogen chloride gas must be supplied to Reactor 2 at the same flow rate as vanadium (II) chloride. The power required to heat incoming hydrogen chloride gas to the temperature of Reactor 2 was found using

$$\dot{Q}_{HRX2,\ HCl} = \dot{n}_{HCl}C_{p,\ HCl}(\overline{T})(T_{RX2} - T_{amb}) \tag{31}$$

where $\dot{n}_{HCl}$ is the molar flow rate of hydrogen chloride gas supplied to Reactor 2, C_p is found at the average temperature between the reactor temperature, T_{RX2}, and ambient temperature, T_{amb}. The amount of power available in the mixture of vanadium (II)

chloride and vanadium (III) chloride is more than that required to heat the incoming

hydrogen chloride gas. The temperature of the vanadium chloride mixture exiting HRX2

was found using

$$T_{O,HRX2} = \frac{\dot{Q}_{HRX2,\,HCl}}{\left[(1-x_d)\dot{n}_{VCl_3}C_{p,\,VCl_3}(\overline{T}) + \dot{n}_{VCl_2}C_{p,\,VCl_2}(\overline{T})\right]} + T_{O,RX2} \qquad (32)$$

where x_d is Reaction 1 conversion efficiency set to 90%, $\dot{n}$ terms are the molar flow rate

from Reactor 1 of each species respectively, C_p terms are the specific heat of each species

respectively at temperature $\overline{T}$, and $\overline{T}$ is the average temperature between the exit

temperature, $T_{O,HRX2}$, and the temperature of the entering vanadium chloride mixture,

$T_{O,RX2}$. The temperature of the vanadium chloride mixture does not fully cool to Reactor

2 temperature. The temperature is further reduced by a precooling unit (Precooler in

FIGURE 1), which releases energy to the surrounding air. The amount of power required

to reduce the temperature to 398 K in the Precooler unit was found using

$$\dot{Q}_{pc,\,VCl_m} = \left[(1-x_d)\dot{n}_{VCl_3}C_{p,\,VCl_3}(\overline{T}) + \dot{n}_{VCl_2}C_{p,\,VCl_2}(\overline{T})\right]\left(T_{RX2} - T_{O,HRX2}\right) \qquad (33)$$

where $\dot{n}$ terms are the molar flow rate of each species, x_d is Reaction 1 conversion

efficiency, C_p is found at the average temperature between the reactor temperature, T_{RX2},

and the HRX2 exiting temperature, $T_{O,HRX2}$. The initial required amount of hydrogen

chloride gas is supplied to storage prior to cycle operation. Some vanadium (II) chloride

and hydrogen chloride gas are left unreacted and pass through the reactor. The flow rate

out of Reactor 2 for vanadium (III) and vanadium (II) chloride were found by

$$\dot{n}_{r2,VCl_3} = x_s\dot{n}_{VCl_2} + (1-x_d)\dot{n}_{VCl_3} \tag{34}$$

$$\dot{n}_{VCl_{2,i}} = (1-x_s)\dot{n}_{VCl_2} \tag{35}$$

where x_s is the conversion efficiency of Reaction 2 equal to 90%, and the vanadium

chloride mixture is recycled to Reactor 1. The flow rate out of Reactor 2 for hydrogen gas

and hydrogen chloride gas was found using

$$\dot{n}_{r2,H_2} = x_s\dot{n}_{VCl_2} \tag{36}$$

$$\dot{n}_{r2,HCl} = (1-x_s)\dot{n}_{HCl} \tag{37}$$

where both products are sent directly to their respective storage vessels after separation.

Reaction 2 releases exothermic energy to the reaction products. The exothermic energy

released by Reaction 2 was found using

$$\Delta H_{RX2}(T) = H_{VCl_3}(T) + \frac{1}{2}H_{H_2}(T) - H_{VCl_2}(T) - H_{HCl}(T) \tag{38}$$

where the enthalpy of each species was found at the temperature of Reaction 2 using

Equations 1, 4, and 6, respectively. Calculated enthalpies for each species are viewed in

TABLE IV.

TABLE IV

ENTHALPIES FOR REACTION 2 SPECIES

Species	Enthalpy (kJ/mole)
$H_2(g)$	2.7549
$HCl(g)$	-89.548
$VCl_2(s)$	-444.89
$VCl_3(s)$	-571.65

Using the enthalpy of each species from TABLE IV in Equation 38, the enthalpy of

reaction for Reaction 2 was calculated as -35.831 kJ/mole. The increased temperature of

Reactor 2 products from the exothermic reaction was found using

$$T_{O,RX2} = (\dot{n}_{VCl_2}\Delta H_{RX2})[\dot{n}_{VCl_{2,i}}C_{p,VCl_2}(\overline{T}) + \dot{n}_{r2,HCl}C_{p,HCl}(\overline{T})$$

$$+ \dot{n}_{r2,VCl_3}C_{p,VCl_3}(\overline{T}) + \dot{n}_{r2,H_2}C_{p,H_2}(\overline{T})]^{-1} + T_{RX2} \qquad (39)$$

where ΔH_{RX2} is the heat of reaction equal to -35.831 kJ/mole, $\dot{n}$ terms are the molar flow

rate of each product species, and C_p is found at the average temperature between Reactor

2, $T_{RX2,}$ and the final temperature of the products, $T_{O,RX2}$. Once $T_{O,RX2}$ is found, multiple

iterations of the system are performed within each time step to solve for $T_{out,VClm}$

(Equation 26) and ΔH_{ph} (Equation 27) to further refine $\dot{n}_{VCl_3}$ (Equation 28).

F. Hydrogen - Chlorine Fuel Cell Simulation

Data from FIGURE 2 was used to evaluate the hydrogen chlorine fuel cell

performance. FIGURE 2 represents theoretical calculations in combination with

experimental losses due to activation energy, hydrogen gas and chlorine gas electrode overpotentials, and membrane resistance overpotential. Data from FIGURE 2 is presented per cm^2 of fuel cell active area. The following calculations were also performed per cm^2 of fuel cell active area.

The fuel cell analysis is performed under the assumption that all reactants and products are cycled without loss. Thus, the stoichiometric fuel cell fuel supply ratio was set to 1.00 for this study. The molar flow rate into the fuel cell of hydrogen gas per active area (mole/s-cm^2) was calculated using

$$\frac{\dot{n}_{H_2}}{A_{active}} = \frac{j\lambda}{nF} \tag{40}$$

where j is the fuel cell operating current density in A/cm^2, A_{active} is the active area of the fuel cell in units of cm^2, λ is the stoichiometric fuel ratio, n is the number of transfer electrons for hydrogen equal to 2, and F is Faraday's constant equal to 96485.3 C/mole.

The incoming hydrogen and chlorine gas is heated from the output hydrogen chloride gas by a counter flow heat recovery heat exchanger (HRX3 in FIGURE 1). The flow rate of hydrogen chloride gas exiting the fuel cell was found using

$$\dot{n}_{HCl,FC} = 2\left(\dot{n}_{H_2}\right) \tag{41}$$

where hydrogen chloride gas is produced according to Equation 12. The total power available, per unit of fuel cell active area, from the hot hydrogen chloride gas exiting the fuel cell (kW/cm^2) was found using

$$\dot{Q}_{HRX3,\ HCl} = \dot{n}_{HCl,FC} C_{p,\ HCl}(\overline{T})(T_{amb} - T_{FC}) \tag{42}$$

where $\dot{n}_{HCl,FC}$ is the molar flow rate of hydrogen chloride gas exiting the fuel cell, and C_p is found at the average temperature between the fuel cell operating temperature, T_{FC}, and ambient temperature, T_{amb}. The temperature of hydrogen gas and chlorine gas exiting HRX3 was found using

$$T_{O,HRX3} = \frac{\dot{Q}_{HRX3,\ HCl}}{\left[\dot{n}_{H_2} C_{p,\ H_2}(\overline{T}) + \dot{n}_{Cl_2} C_{p,\ Cl_2}(\overline{T})\right]} + T_{amb} \tag{43}$$

where $\dot{n}_{H_2}$ and $\dot{n}_{Cl_2}$ are the molar flow rate of hydrogen and chlorine gas entering the fuel cell, which are equal to one another. The energy provided by hydrogen chloride gas exiting the fuel cell is not adequate to fully heat the incoming hydrogen gas and chlorine gas to the fuel cell operating temperature. Since the fuel cell operates independently of the chemical reactors, the additional power required to heat the incoming hydrogen gas and chlorine gas is supplied to Preheater 2 (FIGURE 1) by the fuel cell output. The power (kW/cm^2) required by Preheater 2 was found using

$$\dot{Q}_{ph2} = \left[\dot{n}_{H_2} C_{p,\ H_2}(\overline{T}) + \dot{n}_{Cl_2} C_{p,\ Cl_2}(\overline{T})\right]\left(T_{FC} - T_{O,HRX3}\right) \tag{44}$$

where $\dot{Q}_{ph2}$ is small and supplied by the fuel cell. $\dot{Q}_{ph2}$ is converted to W/cm² for use in

Equation 47.

More chlorine gas is produced from chemical reactions than hydrogen gas.

Therefore, hydrogen gas supply limits the run time of the fuel cell. The amount of

hydrogen gas produced by Reaction 2 was found using

$$n_{H_2} = \dot{n}_{r2,H_2}(t_{step}) \qquad (45)$$

where t_{step} is the time step of the simulations. The total amount of time the fuel cell

operates until the available hydrogen (s-cm²) is depleted was found using

$$t = \frac{n_{H_2}}{\dot{n}_{H_2}} \qquad (46)$$

where n_{H_2} is the total amount of hydrogen gas produced from Reaction 2 in units of

moles, and $\dot{n}_{H_2}$ is the molar flow rate of hydrogen into the fuel cell in units of mole/s-cm².

The total time the fuel cell can operate was converted to units of hr-cm². In order for the

fuel cell to sustain an ongoing reaction in accordance with thermodynamic efficiency,

some of the energy produced is supplied to heat the fuel cell. The total energy produced

by the fuel cell, in W-hr, was found using

$$Q_{out,\,FC} = \left[jE(2 - \eta_{thermo}) - \dot{Q}_{ph2} \right] (t) \qquad (47)$$

34

where j is the current density in A/cm^2, E is the operating voltage of the fuel cell in volts, t is the operating time of the fuel cell in hr-cm^2, and η_{thermo} is the thermodynamic efficiency of the fuel cell operating at 393 K. The thermodynamic efficiency of the fuel cell was calculated using

$$\eta_{thermo} = \left(\frac{\Delta G_{FC}}{\Delta H_{FC}}\right) \tag{48}$$

where the ΔG_{FC} is the Gibbs free energy of the fuel cell reaction calculated from Equation 15, and ΔH_{FC} is the enthalpy of the fuel cell reaction calculated from Equation 13. The thermodynamic efficiency of the fuel cell was equal to 1.039. The total energy output from the fuel cell was compared to the total energy received by the solar collector calculated from Equation 20.

G. Efficiency Parameters

The efficiency of the collector and receiver were calculated with data obtained from the TRNSYS simulations. The total collector and receiver efficiency was calculated using

$$\eta_c = \frac{P_{out,collector}}{P_{in,collector}} \tag{49}$$

$$\eta_r = \frac{P_{out,receiver}}{P_{in,receiver}} \tag{50}$$

where $P_{in,collector}$ is the power the collector receives from incident solar radiation, $P_{out,collector}$ is the power output of the collector to the receiver, $P_{in,receiver}$ is the power input to the receiver from the collector, and $P_{out,receiver}$ is the power out of the receiver to Reactor 1.

The energy efficiency of the chemical reactions that occur in Reactor 1 and Reactor 2 was found using

$$\eta_{RX} = \frac{P_{RX,stored}}{P_{out,\ receiver}} \tag{51}$$

where $P_{RX,stored}$ is the power available in storage from the chemical reactions, and $P_{out,receiver}$ is the power output of the receiver to Reactor 1.

The total efficiency of the fuel cell was found using

$$\eta_{FC} = \left(\frac{Q_{out,FC}}{n_{H_2}\Delta H_{FC}} \right) \tag{52}$$

where $Q_{out,FC}$ is the total energy output of the fuel cell (Equation 47), n_{H_2} is the amount of reactants supplied in kmol, and ΔH_{FC} is the fuel cell enthalpy (Equation 13). Equation 52 characterizes the total fuel cell cycle efficiency, which includes the efficiency reduction from electrical energy supplied to Preheater 2.

The total efficiency of the system is characterized by

$$\eta_{overall} = \eta_c \eta_r \eta_{RX} \eta_{FC} \tag{53}$$

where η_c is the collector efficiency, η_r is the receiver efficiency, η_{RX} is the chemical reaction efficiency, and η_{FC} is the fuel cell efficiency. The efficiency of the system was evaluated within each time step of the simulation. Alternatively, the efficiency of the system can be characterized by comparing the net electrical energy output from the fuel cell directly to the solar energy input to the collector. The energy input to the solar collector was found using

$$Q_{in,\,collector} = P_{in,\,collector}\, t_{step} \tag{54}$$

where $P_{in,\,collector}$ was found using Equation 20 and is in units of Watts, and t_{step} is the time step of the simulation equal to 0.25 hr. The overall efficiency of the system is then

$$\eta_{overall} = \frac{Q_{out,\,FC}}{Q_{in,\,collector}} \tag{55}$$

where $Q_{out,\,FC}$ was found using Equation 47 and $Q_{in,\,collector}$ was found using Equation 54. The efficiency calculated from Equation 55 is equivalent to that from Equation 53. The system efficiency was evaluated for each time step of the simulation and is reported for a yearly and monthly period in the results section.

IV.   SIMULATION PLAN

The vanadium chloride cycle efficiency for short-term storage was evaluated and compared on a monthly and yearly basis. The comparison was performed for two fuel cell operating current densities, 0.039 A/cm^2 and 0.085 A/cm^2, two Reaction 2 conversion efficiencies, 45% and 90%, and in two different locations, Louisville, KY and Phoenix, AZ. To gain a better understanding of how Reaction 2 conversion efficiency effects the overall system efficiency, system efficiency was also calculated for a wider range of Reaction 2 conversion efficiency from 0% to 90% for the same two fuel cell current densities and two locations.

The cumulative efficiency of vanadium chloride (VCl$_3$) cycle was compared to that of thermal energy storage (TES), compressed air energy storage systems (CAES), vanadium flow battery (Battery), pumped hydro electrical storage (PHES), and thermochemical ammonia storage (NH$_3$) systems. These energy storage and conversion systems were evaluated by Shakeri et al. (2014). TES, CAES, Battery, PHES, and NH$_3$ storage systems utilized a Stirling engine for electrical energy output. All systems used the same parabolic dish collector to obtain energy from incident beam radiation. The Stirling engine was responsible for the largest drop in efficiency of the other storage systems (Shakeri, Soltanzadeh et al. 2014).

A long-term energy storage comparison between the vanadium chloride cycle and the other systems was performed for seven months of continuous storage. The vanadium chloride cycle, operating with a fuel cell current density of 0.039 A/cm^2 and 0.085 A/cm^2 and a Reaction 2 conversion efficiency of 90%, was compared to the other systems in Phoenix, Arizona, and Louisville, Kentucky.

V.   RESULTS

A. Short - Term Energy Storage Efficiency

The peak efficiency of the system was higher in Phoenix than in Louisville for fuel cell operation at 0.039 A/cm^2 and 0.085 A/cm^2 as viewed in FIGURE 4.
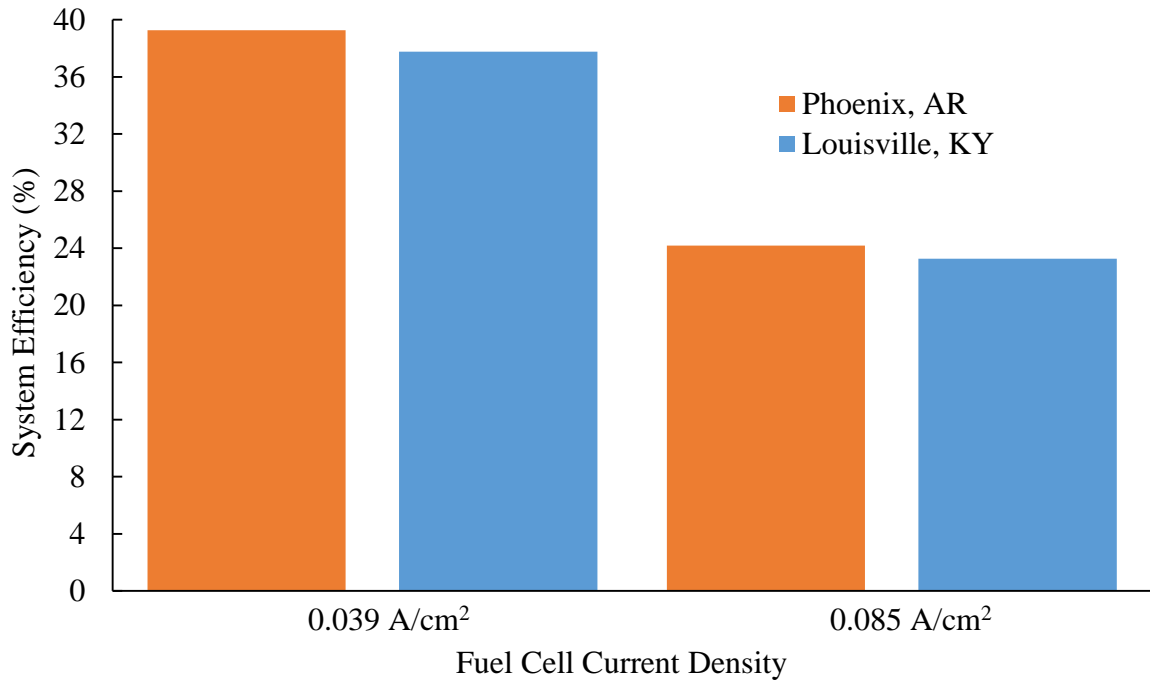

FIGURE 4 - Yearly System Efficiency For Two Fuel Cell Current Densities

Operating the fuel cell with a higher current density reduced system efficiency in both Louisville and Phoenix.

The system efficiency for Phoenix and Louisville as a function of Reaction 2 (Equation 11) conversion efficiency for fuel cell operation at 0.039 A/cm^2 and 0.085 A/cm^2 is viewed in FIGURE 5.
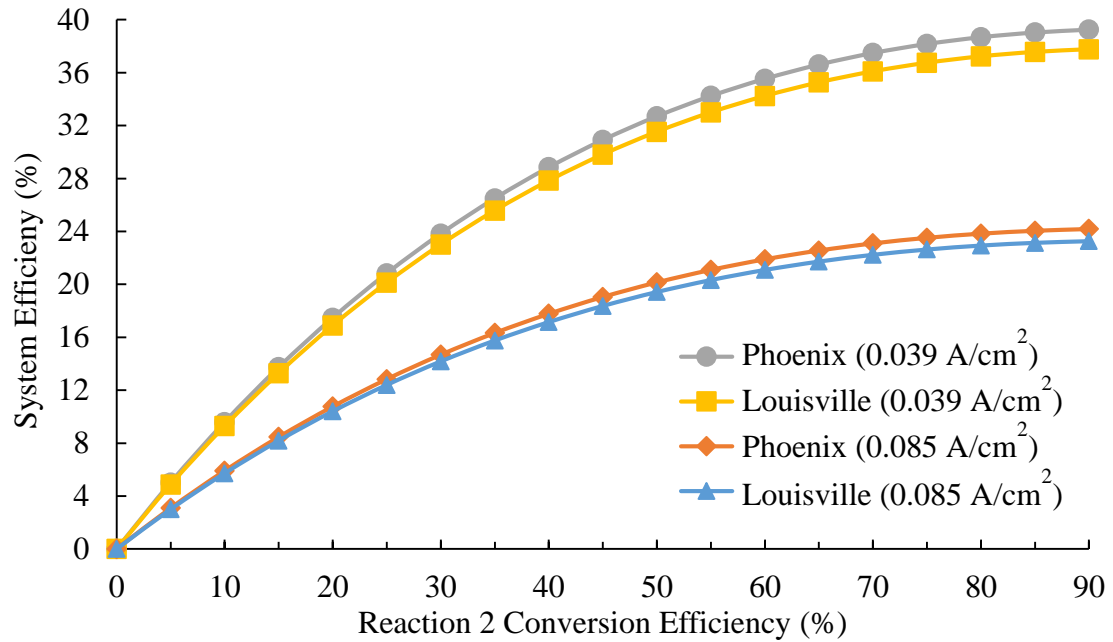
FIGURE 5 - System Efficiency For Various Reaction 2 Conversion Efficiencies

The system efficiency was higher in Phoenix than in Louisville while varying the conversion efficiency of Reaction 2.

The monthly efficiency of the system, operating with a Reaction 2 (Equation 11) conversion efficiency of 90%, and fuel cell operation at 0.039 A/cm^2 and 0.085 A/cm^2, is viewed in FIGURE 6.
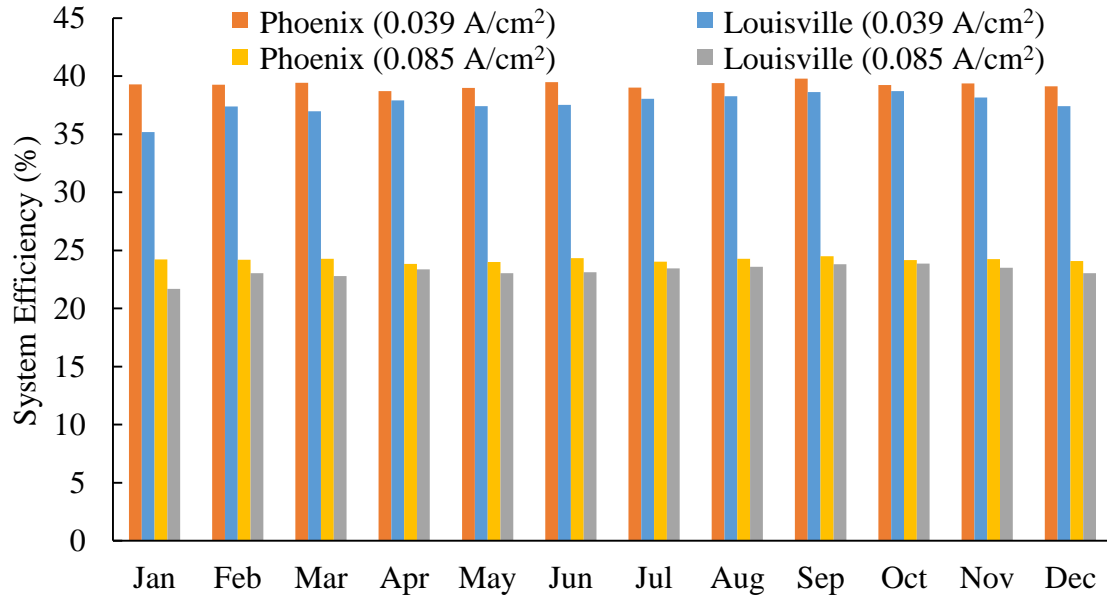
FIGURE 6 - Monthly Efficiency For 90% Reaction 2 Conversion Efficiency

The monthly efficiency is higher in Phoenix than Louisville for every month of the year and for both fuel cell operating current densities.

The monthly efficiency of the system, operated with a Reaction 2 (Equation 11) conversion efficiency of 45% and fuel cell operation at 0.039 A/cm^2 and 0.085 A/cm^2, is viewed in FIGURE 7.
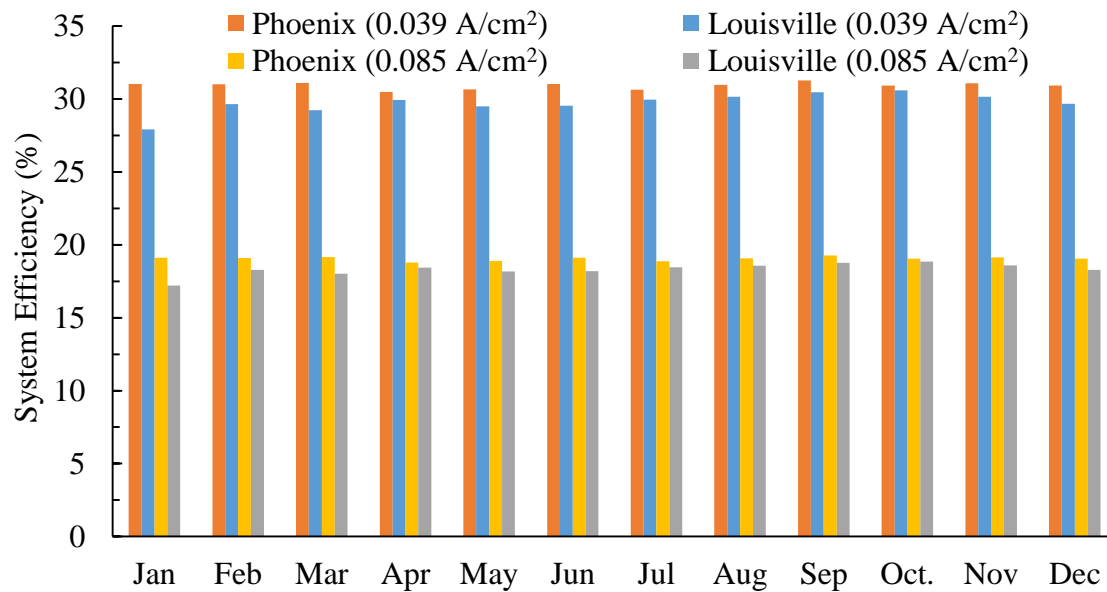

FIGURE 7 - Monthly Efficiency For 45% Reaction 2 Conversion Efficiency

The monthly efficiency of the system operating with a conversion efficiency of 45% for Reaction 2 is lower in Louisville when compared to Phoenix. Phoenix has a higher efficiency for both fuel cell current densities.

<u>B. Cumulative System Efficiency</u>

The cumulative efficiency at different stages for the VCl_3 system, with a fuel cell current density of 0.039 A/cm^2, compared to thermal energy storage (TES), compressed air energy storage systems (CAES), vanadium flow battery (Battery), pumped hydro electrical storage (PHES), and thermochemical ammonia storage (NH_3) systems for Louisville, KY and Phoenix, AZ is viewed in FIGURE 8 and FIGURE 9, respectively.
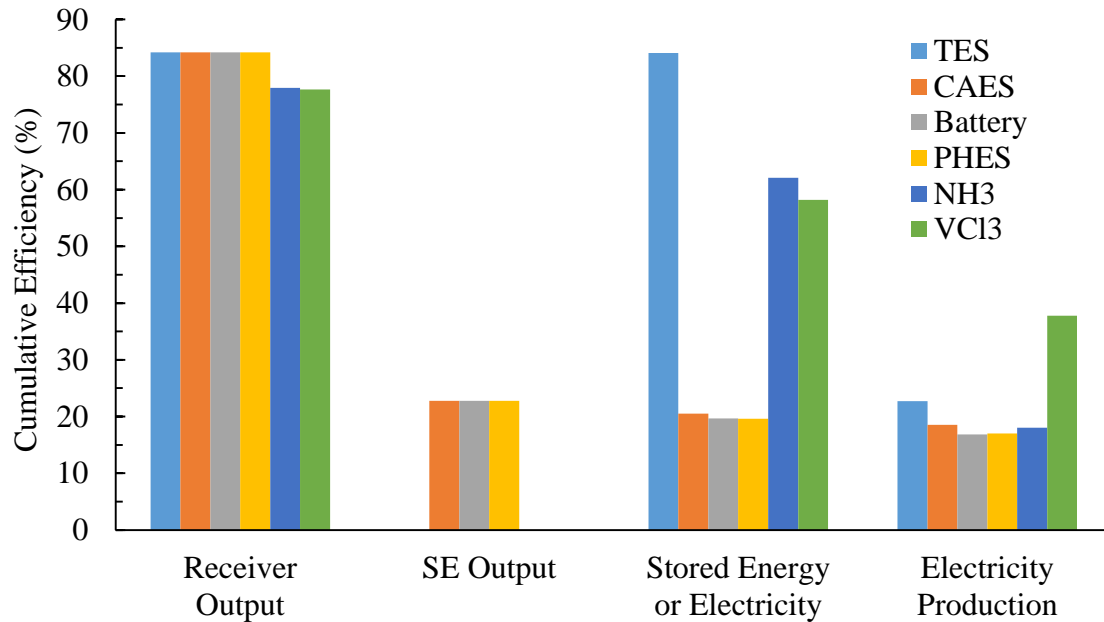

FIGURE 8 - Cumulative Storage Efficiency For 0.039 A/cm^2 in Louisville, KY

FIGURE 9 - Cumulative Storage Efficiency For 0.039 A/cm^2 in Phoenix, AZ

TES, CAES, Battery, PHES, and NH$_3$ storage systems were evaluated with Stirling engine electrical energy production by Shakeri et al. (2014). For comparison, a fuel cell operating current density of 0.039 A/cm^2 and a Reaction 2 conversion efficiency of 90% were used for FIGURE 8 and FIGURE9.

The cumulative efficiency at different stages for the VCl$_3$ system, with a fuel cell current density of 0.085 A/cm^2, compared to the other storage systems in Louisville, KY and Phoenix, AZ is viewed in FIGURE 10 and FIGURE 11, respectively.

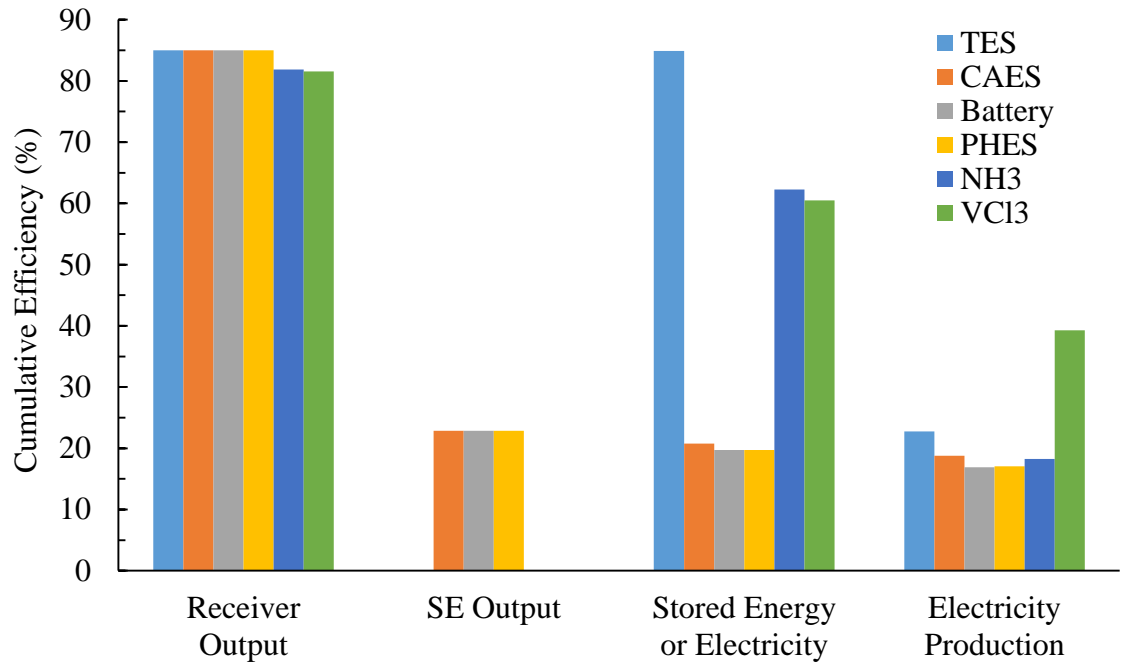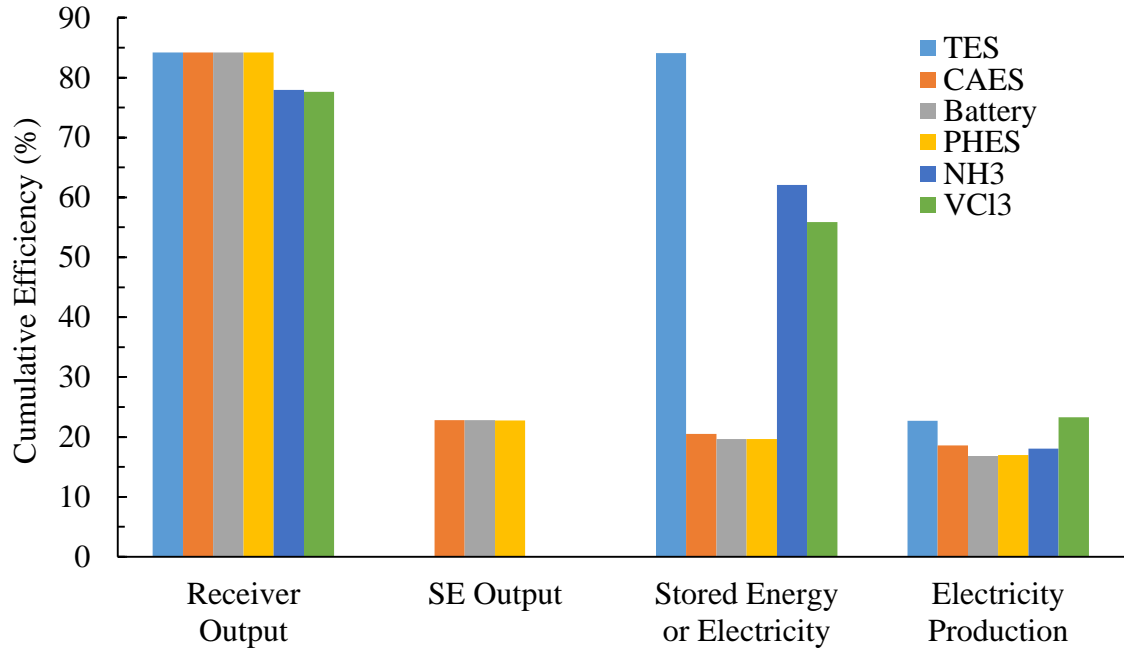FIGURE 10 - Cumulative Storage Efficiency For 0.085 A/cm2 in Louisville, KY
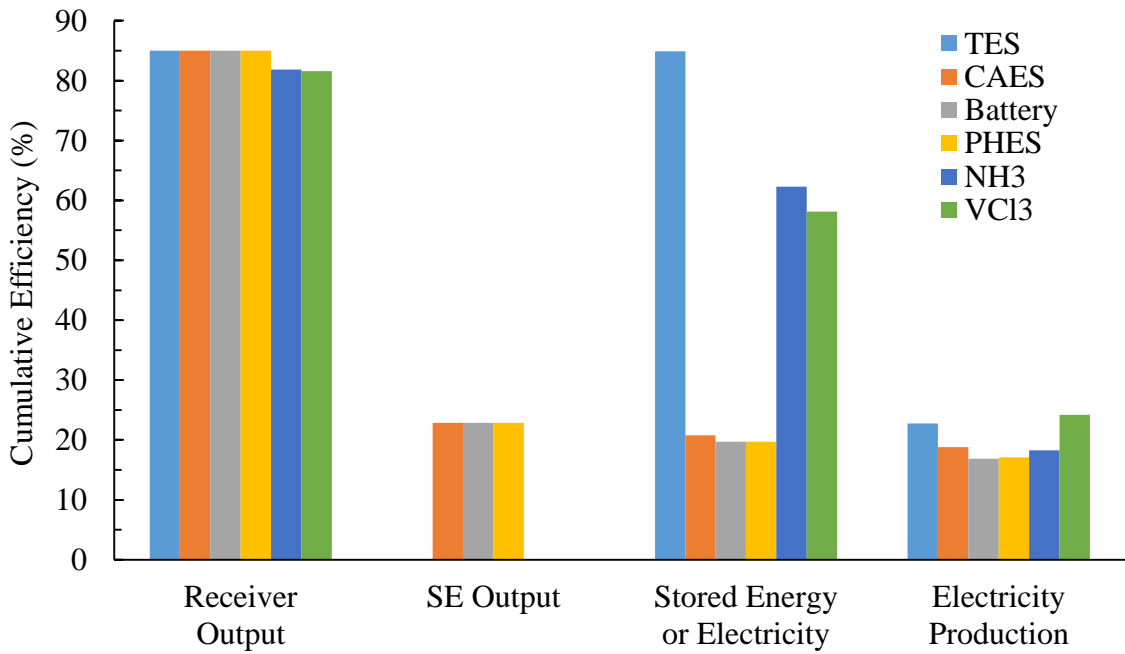
FIGURE 11 - Cumulative Storage Efficiency For 0.085 A/cm2 in Phoenix, AZ

A fuel cell operating current density of 0.085 A/cm^2 and a Reaction 2 conversion

efficiency of 90% were used for FIGURE 10 and FIGURE 11.

C. Long - Term Energy Storage Efficiency

A comparison of long-term energy storage efficiency of the systems in Louisville, KY and Phoenix, AZ for fuel cell operation at 0.039 A/cm^2 is viewed in FIGURE 12 and FIGURE 13, respectively.

FIGURE 12 – Long-Term Efficiency For 0.039 A/cm^2 Louisville, KY

FIGURE 13 – Long-Term Efficiency For 0.039 A/cm^2 Phoenix, AZ

FIGURE 12 and FIGURE 13 correspond to the VCl_3 system operating with a 90%
conversion efficiency for Reaction 2. All other system used a Stirling engine for energy
production (Shakeri, Soltanzadeh et al. 2014).

A comparison of long-term energy efficiency of the systems in Louisville, KY and
Phoenix, AZ for fuel cell operation at 0.085 A/cm^2 is viewed in FIGURE 14 and
FIGURE 15, respectively.

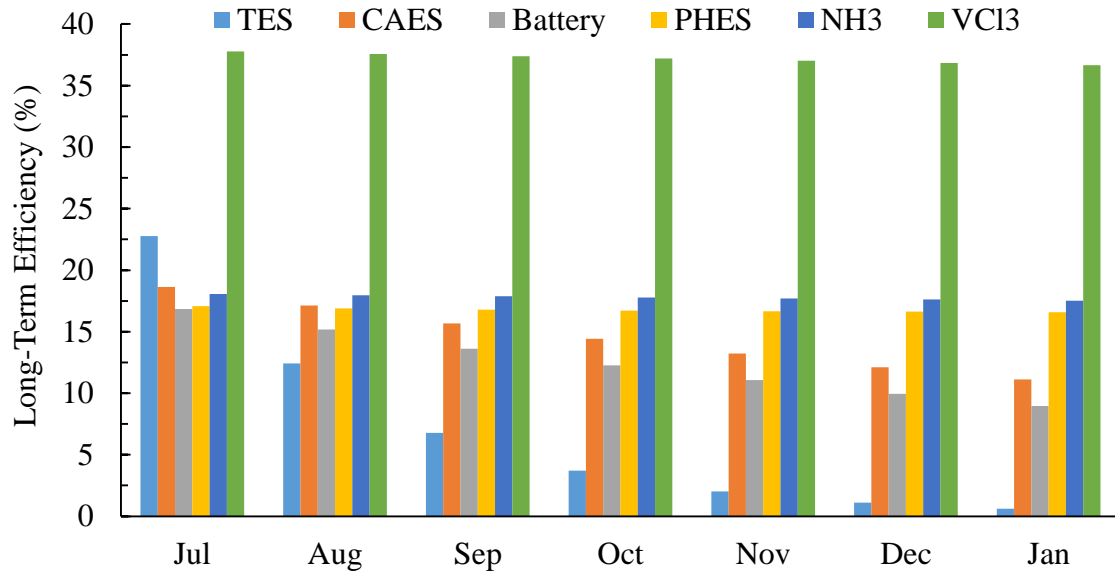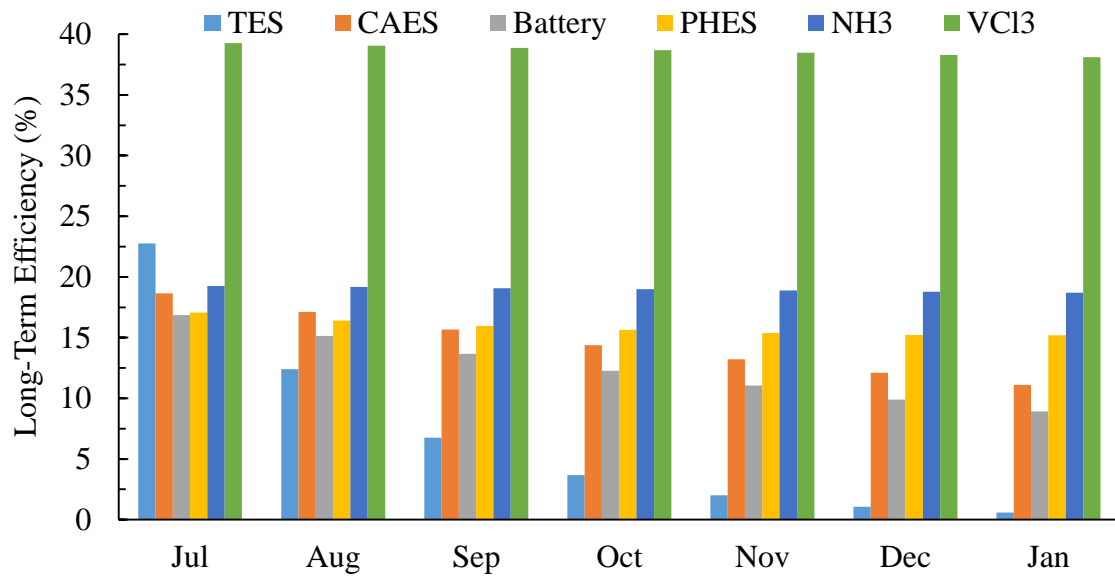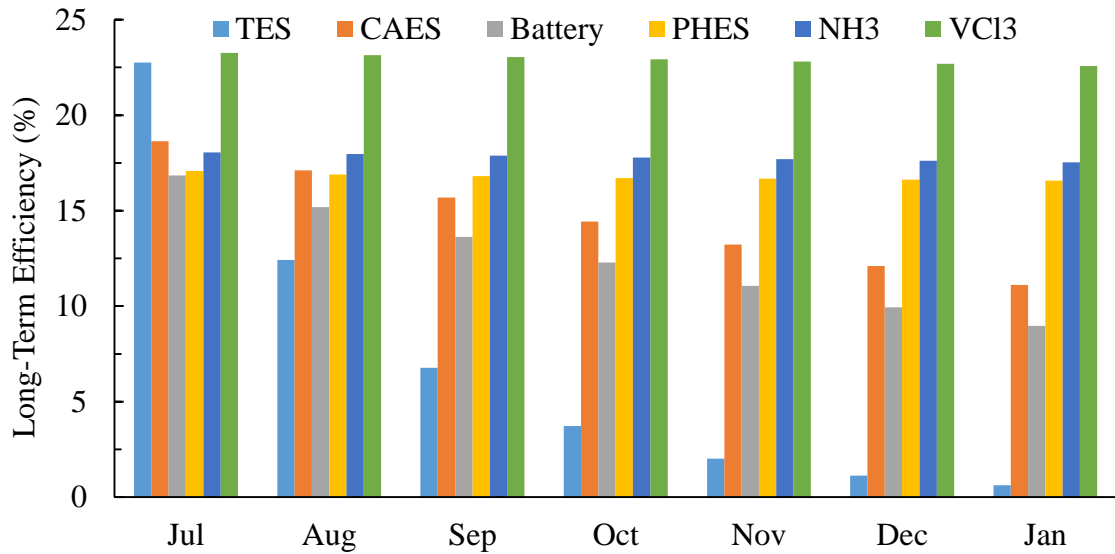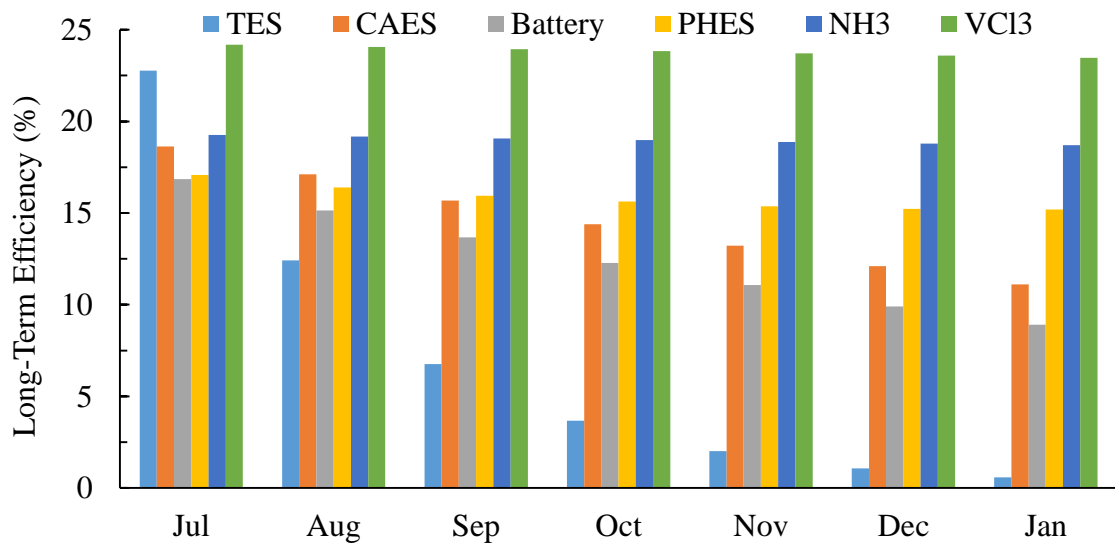FIGURE 14 – Long-Term Efficiency For 0.085 A/cm^2 Louisville, KY

FIGURE 15 – Long-Term Efficiency For 0.085 A/cm^2 Phoenix, AZ

FIGURE 14 and FIGURE 15 correspond to the VCl_3 system operating with a 90%

conversion efficiency for Reaction 2. All other system used a Stirling engine for energy

production (Shakeri, Soltanzadeh et al. 2014).

VI.   DISCUSSION

A. Short - Term Energy Storage Efficiency

As seen in FIGURE 4, the VCl_3 system achieved a higher efficiency with the fuel cell operating at 0.039 A/cm^2 than operation at 0.085 A/cm^2. For fuel cell operation at 0.039 A/cm^2, efficiency in Louisville was 37.8% and efficiency in Phoenix was 39.3%. For fuel cell operation at 0.085 A/cm^2, Louisville had an efficiency of 23.3% and Phoenix had an efficiency of 24.2%. The efficiency in Louisville, KY was only slightly lower than the efficiency in Phoenix, AZ for both fuel cell current densities. Parabolic dish collectors operate at a higher efficiency in Phoenix than Louisville. The change in collector and receiver efficiency between Phoenix and Louisville results in a lower efficiency for the VCl_3 system operating in Louisville.

The conversion efficiency of Reaction 2 (Equation 11) significantly effects the energy storage efficiency. As previously stated, conversion efficiency for Reaction 2 has not been characterized. FIGURE 5 shows the system efficiency as a function of the conversion efficiency of Reaction 2 for a temperature of 398 K. System efficiency decreases rapidly when Reaction 2 conversion efficiency is below 45%. It is expected that the conversion efficiency for Reaction 2 will be lower than 90%. Introducing catalysts to the reaction would substantially improve the conversion efficiency, possibly as high as 90%, corresponding to a higher overall system efficiency (Amendola 2010). The use of a catalyst is assumed with an operation conversion efficiency of 90%. As the conversion efficiency of Reaction 2 increases, the amount of exothermic energy released is higher. The exothermic energy is released to the products of Reactor 2. When Reactor

2 products are recycled to Reactor 1, the increase in temperature from the exothermic energy released results in a smaller amount of solar energy used in Preheater 1. More solar energy is capable of being used for Reaction 1, increasing the overall system efficiency. For a fuel cell operating current density of 0.039 A/cm^2 and a Reaction 2 conversion efficiency of 45%, system efficiency in Phoenix and Louisville dropped to 30.9% and 29.8%, respectively. For fuel cell operating current density of 0.085 A/cm^2 and a Reaction 2 conversion efficiency of 45%, system efficiency in Phoenix and Louisville dropped to 19.1% and 18.4%, respectively.

The effect of conversion efficiency and fuel cell operation at both 0.039 A/cm^2 and 0.085 A/cm^2 fuel cell current densities is viewed, respectively, in FIGURE 6 and FIGURE 7 for each month of the year. The monthly efficiency in Phoenix was higher than in Louisville for both fuel cell operating cases. When using a Reaction 2 conversion efficiency of 45%, the overall system efficiency was reduced by around 8% for fuel cell operation at 0.039 A/cm^2 and around 5% for fuel cell operation at 0.085 A/cm^2 for both locations. As previously mentioned, adding a catalyst to the reaction could increase the conversion efficiency substantially. In addition, the system efficiency in Phoenix varied a smaller amount from month-to-month while in Louisville, the system efficiency varied a larger amount. System efficiencies were higher in the summer months and lower during the winter months in Louisville. The variance in system efficiency for Louisville was a result of the collector and receiver efficiency. Cooler weather in Louisville caused a lower receiver efficiency.

As viewed in FIGURE 6 and FIGURE 7, operating the fuel cell at 0.085 A/cm^2 resulted in a further loss in system efficiency. There was around 12% decrease in system

49

efficiency from fuel cell operation at 0.039 A/cm^2 to 0.085 A/cm^2 for both Phoenix and Louisville with a Reaction 2 conversion efficiency of 45%. There was around 15% decrease in system efficiency from fuel cell operation at 0.039 A/cm^2 to 0.085 A/cm^2 with a Reaction 2 conversion efficiency of 90%. The fuel cell efficiency reduced from 64.9% for a current density of 0.039 A/cm^2 to 40.0% for 0.085 A/cm^2. Operating the fuel cell at a lower current density resulted in higher system efficiency.

Sub-optimal operating conditions were defined as a Reaction 2 conversion efficiency of 45%, a fuel cell current density of 0.085 A/cm^2, and operation in Louisville. Optimal operating conditions were defined as a Reaction 2 conversion efficiency of 90%, a fuel cell current density of 0.039 A/cm^2, and operation in Phoenix. As seen in FIGURE 6 and FIGURE 7, overall short-term energy storage efficiencies for the VCl_3 cycle varied from 17.2% to 18.8% for sub-optimal operating conditions and 38.7% to 39.8% for optimal operating conditions. The short-term energy storage potential of the system is relatively high and shows a competitive advantage when compared to other energy storage systems.

B. Cumulative System Efficiency

The VCl_3 system was compared to TES, CAES, Battery, PHES, and NH_3 storage methods in FIGURE 8 and FIGURE 9. The battery, CAES, and PHES systems used the Stirling engine for energy production prior to storage, shown in the second group of bars. The TES and NH_3 systems used the Stirling engine to produce electrical energy at the end of the cycle resulting in a higher efficiency in storage of energy than CAES, Battery, and

PHES, corresponding to the third group of bars. VCl_3 storage efficiency is lower due to the efficiency of the chemical reactions as seen in FIGURE 8 and FIGURE 9. A smaller efficiency of energy storage is achieved by the VCl_3 cycle. CAES and PHES systems require caverns and reservoirs, respectively, in close proximity to the electric generation plant. Although transmission lines can be used, transport over long distances is undesirable. NH_3, vanadium flow batteries, and the VCl_3 cycle use thermochemical storage in conventional tanks. Thus, these systems can be implemented anywhere where acreage and sun exposure are available (Shakeri, Soltanzadeh et al. 2014). The fourth group of bars corresponds to the overall efficiency of electrical energy production of each system.

The VCl_3 cycle was compared in FIGURE 8 and FIGURE 9 for a Reaction 2 conversion efficiency of 90% and with fuel cell operation at 0.039 A/cm^2. It is clear from FIGURE 8 and FIGURE 9 that the VCl_3 system displays a significant advantage over the other storage systems. Although the VCl_3 system has lower storage efficiency than the NH_3 and TES systems, the efficiency of energy production from the hydrogen – chlorine fuel cell is higher than Stirling engine energy production. High fuel cell efficiency resulted in a higher efficiency in converting stored energy to electrical energy, yielding a higher overall system efficiency. In addition, the VCl_3 system is capable of storing energy for long periods of time without significant losses. Although the NH_3 system can also store energy indefinitely, the VCl_3 system displays a higher electric conversion efficiency, giving it the overall advantage. The yearly system efficiency for fuel cell operation at 0.039 A/cm^2 was 39.3% in Phoenix and 37.8% in Louisville as seen in

FIGURE 8 and FIGURE 9, respectively. The VCl$_3$ cycle displayed an overall efficiency 16.5% higher than the TES system in Phoenix, and 15.1% higher than TES in Louisville.

Operating the fuel cell with a higher current density resulted in a significant decrease in efficiency as previously discussed. As seen in FIGURE 10 and FIGURE 11, the yearly system efficiency for fuel cell operation at 0.085 A/cm^2 was 24.2% in Phoenix and 23.3% in Louisville, which is still competitive with TES at around 22.7% for both locations. Additionally, the VCl$_3$ system gains a significant advantage over TES by storing energy efficiently for long periods of time discussed further in the next section. In a location with a primarily cloudy climate, multiday storage grows increasingly important for energy production where the VCl$_3$ system displays an advantage.

C. Long - Term Energy Storage Efficiency

The long-term energy storage comparison for all storage systems in Louisville and Phoenix, where the VCl$_3$ cycle operates with a fuel cell current density of 0.039 A/cm^2 and conversion efficiency of 90%, is viewed in FIGURE 12 and FIGURE 13, respectively. These figures show a large advantage of long-term energy storage with the VCl$_3$ system when compared to the other storage methods. The VCl$_3$ system had the largest initial efficiency of all the systems, followed by TES, NH$_3$, and CAES storage systems. After one month, the efficiency of the TES system fell below the efficiency of the NH$_3$ system. CAES efficiency fell below NH$_3$ efficiency after two months in Louisville. In Phoenix, CAES efficiency was consistently lower than the NH$_3$ efficiency. Losses from the PHES system were primarily through evaporation, which varied from

0.3% to 0.8% in Louisville and 0.5% to 3.8% in Phoenix (Shakeri, Soltanzadeh et al. 2014). The efficiency of the CAES system fell below the efficiency of the PHES system after three months. The VCl_3 and NH_3 systems had a higher efficiency for long-term storage than all other systems with the VCl_3 system being around 19.2% higher than the NH_3 system. The VCl_3 system operating with a fuel cell current density of 0.039 A/cm^2 offered a clear advantage over the NH_3 system.

The long-term energy storage comparison for all storage systems in Louisville and Phoenix, where the VCl_3 system operates with a fuel cell current density of 0.085 A/cm^2 and Reaction 2 conversion efficiency of 90%, is viewed in FIGURE 14 and FIGURE 15, respectively. The TES system initially has lower storage efficiency than the VCl_3 system. The TES storage efficiency fell below the NH_3 storage efficiency after one month. CAES efficiency fell below NH_3 efficiency after two months in Louisville. In Phoenix, CAES efficiency was consistently lower than the NH_3 efficiency. The CAES storage efficiency fell below PHES after three months in Louisville and Phoenix. Efficiency using the VCl_3 system was consistently higher than efficiency using the NH_3 system. Although the VCl_3 system operating with a fuel cell current density of 0.085 A/cm^2 displayed a lower efficiency, the VCl_3 system efficiency remained higher than the NH_3 cycle in both Louisville and Phoenix. The VCl_3 cycle, operating with a fuel cell current density of 0.085 A/cm^2, displayed around 5.0% higher efficiency than the NH_3 in both Louisville and Phoenix. Despite operating with a fuel cell current density of 0.085 A/cm^2, the VCl_3 system displayed advantages over all other storage systems.

VII.   CONCLUSIONS

Energy storage using the VCl_3 cycle was analyzed and compared to five other energy storage systems. With the caveat that the kinetics of Reaction 1 (Equation 10) and Reaction 2 (Equation 11) are not well-characterized, the efficiency of the VCl_3 system displays potential advantages over other energy conversion and storage methods. Low conversion efficiency for Reaction 2 was found to have a large impact on the efficiency. But, a Reaction 2 conversion efficiency above 45% was found to have a small impact on the VCl_3 system efficiency. Collector and receiver efficiency had a large effect on the overall efficiency of each system. Receiver temperature is a key factor in the overall efficiency of the energy storage systems. Climate conditions had a small effect on system efficiency. Operation in the cloudy Midwest United States was only slightly less efficient than in the sunnier Southwest.

Thermochemical energy storage systems were found to have a key advantage over other storage systems in their ability to store energy over long periods of time with small losses. The NH_3 storage system displayed a lower operating efficiency and storage efficiency than the VCl_3 system in Louisville and Phoenix for both fuel cell operating current densities. For long-term storage periods, the VCl_3 storage system displayed higher efficiency than NH_3, TES, CAES, vanadium flow battery, and PHES storage systems.

VIII. RECOMMENDATIONS

Component design for the vanadium chloride system has not yet been completed. Additional work on the system details and design would help gain insight on the achievable efficiency of the system. The reaction kinetics, including conversion efficiency and reaction rate, of Reactions 1 and 2 require quantification to confidently characterize the efficiency of the system. Parabolic trough collectors offer a distinct economic advantage due to their low cost. Currently, trough collectors are not capable of reaching the high temperatures required for VCl_3 decomposition at high conversion efficiencies (Fernández-García, Zarza et al. 2010), but design improvements to increase performance may make their use feasible. Additional research into catalysts for both Reaction 1 and 2 may reduce reactor temperature and increase the efficiency of the system (Amendola 2010). There is little research on dry hydrogen – chlorine fuel cells. A more accurate model of the dry hydrogen – chlorine fuel cell is necessary to fully characterize the efficiency of the VCl_3 system. A large amount of the exothermic energy released from Reaction 2 is lost. Methods to retain or convert this energy would increase the overall efficiency of the VCl_3 system. An analysis of the losses from the reactor vessels, piping, and fuel cell should be performed. Methods of retaining the thermal energy that is lost to the surroundings by chlorine gas, hydrogen gas, and hydrogen chloride gas should be researched. Short-term thermal storage is one option for retaining this energy. Because the VCl_3 cycle has higher overall efficiency than direct conversion of solar energy to electricity in a Stirling engine, it presents a high-performance alternative for immediate solar-electric production as well. The high performance of the vanadium chloride system over a range of storage durations precludes the need to

evaluate a combination of short and long-term energy storage and production systems to maximize efficiency at the utility scale.

REFERENCES CITED

Amendola, S. (2010). U.S. Patent 7,799,315.

Fernández-García, A., et al. (2010). "Parabolic-trough solar collectors and their applications." Renewable and Sustainable Energy Reviews **14**(7): 1695-1721.

Funk, J. E. (1976). "Thermochemical production of hydrogen via multistage water splitting processes." International Journal of Hydrogen Energy **1**(1): 33-43.

Harvey, L. D. D. (1995). "Solar-hydrogen electricity generation in the context of global CO2 emission reduction." Climatic Change **29**(1): 53-89.

Harvey, L. D. D. (1996). "Solar-hydrogen electricity generation and global CO2 emission reduction." International Journal of Hydrogen Energy **21**(7): 583-595.

Huskinson, B., et al. (2014). "A metal-free organic-inorganic aqueous flow battery." Nature **505**(7482): 195-198.

King, E. G. (1948). "Heat Contents at High Temperatures of Vanadium Dichloride and Vanadium Trichloride." Journal of the American Chemical Society **70**(6): 2154-2155.

Klein et al. (2004). TRNSYS 16: A Transient System Simulation Program. University of Wisconsin, Madison, USA, Solar Energy Laboratory.

Knoche, K. F. and P. Schuster (1984). "Thermochemical production of hydrogen by a vanadium/chlorine cycle. Part 1: An energy and exergy analysis of the process." International Journal of Hydrogen Energy **9**(6): 457-472.

Lewis, M. A. and J. G. Masin (2009). "The evaluation of alternative thermochemical cycles – Part II: The down-selection process." International Journal of Hydrogen Energy **34**(9): 4125-4135.

Liu, S., et al. (2013). "Nonhumidified high temperature H2/Cl2 fuel cells using protic ionic liquids." Journal of Materials Chemistry A **1**(14): 4423-4426.

Microsoft (2013). Microsoft Excel. Redmond, Washington, Microsoft.

National Institute of Standards and Technology (2005). <u>NIST Chemistry WebBook, NIST Standard Reference Database Number 69</u>, National Institute of Standards and Technology.

National Renewable Energy Laboratory (2015). "National Solar Radiation Data Base." Retrieved 14 Jan, 2015, from http://rredc.nrel.gov/solar/old_data/nsrdb/1991-2005/tmy3/.

Rugolo, J., et al. (2012). "Model of Performance of a Regenerative Hydrogen Chlorine Fuel Cell for Grid-Scale Electrical Energy Storage." <u>J. Electrochem. Soc.</u> **159**(B133).

Rugolo, J. S. (2011). Electricity Storage and the Hydrogen-Chlorine Fuel Cell. Ann Arbor, Harvard University. **3446168:** 249-n/a.

Shakeri, M., et al. (2014). "Efficiency of Solar Electricity Production With Long-Term Storage." <u>Journal of Solar Energy Engineering</u> **137**(1): 011007-011007.

Simons, J. H. and M. G. Powell (1945). "Properties of Vanadium Tetrachloride." <u>Journal of the American Chemical Society</u> **67**(1): 75-77.

Stewart, F. F. (2007). Separations Needs for the Alternate Chemical Cycles**:** Medium: ED.

Stuetzle, T. A. (2002). <u>Automatic Control of the 30 MWe SEGS VI Parabolic Trough Plant</u>, University of Wisconsin--Madison.

Thomassen, M., et al. (2006). "A computational simulation of a hydrogen/chlorine single fuel cell." <u>Journal of Power Sources</u> **157**(1): 271-283.

U.S. Energy Information Administration (2012). "Primary Energy Consumption by Source and Sector." Retrieved 23 Jan, 2015, from http://www.eia.gov/totalenergy/data/monthly/pdf/flow/primary_energy.pdf.

U.S. Energy Information Administration (2013). "How much U.S. electricity is generated from renewable energy?". Retrieved 15 March, 2015, from http://www.eia.gov/energy_in_brief/article/renewable_electricity.cfm.

Wikipedia Contributors (2015). "Coulomb." Retrieved March 15, 2015, from http://en.wikipedia.org/w/index.php?title=Coulomb&oldid=653895284.

Yajima, A., et al. (1979). "The thermal decomposition of vanadium(III) chloride oxide and its reaction with oxygen." <u>Bulletin of the Chemical Society of Japan</u> **52**(11): 3292-3295.

Yajima, A., et al. (1980). "The preparation of vanadium tetrachloride from vanadium dichloride oxide and vanadium trichloride and the hydrogen reduction process of vanadium tetrachloride." <u>Bulletin of the Chemical Society of Japan</u> **53**(10): 2843-2846.

VITA

Caleb Rogers was born in Columbus, Ohio. He moved to Cincinnati at age nine and began attended St. Xavier High School when he was age 14. At age 16, he relocated to Louisville, Kentucky and attended Christian Academy of Louisville where he received his high school diploma.

He began to study mechanical engineering at the University of Louisville J.B. Speed School of Engineering in August of 2009. Caleb graduated with his bachelor's degree in mechanical engineering in December of 2014 at which point, he decided to pursue a master of engineering degree in mechanical engineering at the University of Louisville. He received his master of engineering degree in mechanical engineering May of 2015.